isvr Institute of Sound and Vibration Research

Contact Filters in Wheel/Rail Noise Prediction

R. Ford and D.J. Thompson

ISVR Technical Memorandum 907

April 2003

University of Southampton

SCIENTIFIC PUBLICATIONS BY THE ISVR

Technical Reports are published to promote timely dissemination of research results by ISVR personnel. This medium permits more detailed presentation than is usually acceptable for scientific journals. Responsibility for both the content and any opinions expressed rests entirely with the author(s).

Technical Memoranda are produced to enable the early or preliminary release of information by ISVR personnel where such release is deemed to the appropriate. Information contained in these memoranda may be incomplete, or form part of a continuing programme; this should be borne in mind when using or quoting from these documents.

Contract Reports are produced to record the results of scientific work carried out for sponsors, under contract. The ISVR treats these reports as confidential to sponsors and does not make them available for general circulation. Individual sponsors may, however, authorize subsequent release of the material.

UNIVERSITY OF SOUTHAMPTON

INSTITUTE OF SOUND AND VIBRATION RESEARCH

DYNAMICS GROUP

Contact Filters in Wheel/Rail Noise Prediction

by

R. Ford and D.J. Thompson

ISVR Technical Memorandum No: 907

April 2003

Authorised for issue by
Professor M.J. Brennan
Group Chairman

ABSTRACT

When predicting wheel/rail rolling noise due to wheel and rail roughness a "contact filter" is generally applied to account for the effect of the finite size of the wheel/rail contact. Various representations of the filter have been devised, but when the analysis is required in the time-domain the calculations for this contact filter must be quick.

In order to produce a versatile and relatively quick representation of the contact filter, Remington and Webb developed a three-dimensional 'Distributed Point Reacting Spring' (DPRS) model of the contact. However, if only one line of data is available this is too complex and for this reason a simpler, two-dimensional version has been developed and is described here. Questions arise as to the validity of these simplified models, particularly when applied to geometric features such as large amplitude roughness, wheel flats and rail joints. To assess their three-dimensional DPRS model, Remington and Webb developed a Boussinesq analysis of the contact filter. This, although slow, provides a more comprehensive analysis for purposes of comparison. A similar Boussinesq analysis has been implemented in Matlab for this work and used to evaluate the two-dimensional DPRS model. The results in one-third octave bands were found to agree within 3 dB.

Results suggest that the two-dimensional DPRS model may well have a wider range of applicability than might have been expected, even on features such as large amplitude sinusoidal roughness and discrete features such as a rail joint. It is also shown that a simple windowing of roughness data can provide useful and instructive results.

It is shown that the filter effect for a dipped rail joint, while differing considerably from the frequency-domain effect calculated using sinusoidal roughness, can nevertheless be adequately modelled by the 2-D mattress model. The mattress model has also been implemented in a time-domain wheel/rail interaction model. This gives similar results to the quasi-static roughness filtering for moderate roughness, but the dynamic effects are significant when the roughness amplitudes are large, including the case of dipped rail joints.

ACKNOWLEDGMENTS

The work described has been partly carried out during the sabbatical leave of the first author from University of New South Wales, Sydney, Australia between July 2002 and January 2003. The context for the work was the project 'Non-linear Effects at the Wheel/rail Interface and their Influence on Noise Generation', grant GR/M82455, supported by EPSRC (Engineering and Physical Sciences Research Council of the United Kingdom).

CONTENTS

1 INTRODUCTION

When analysing the generation of rolling noise due to wheel and rail roughness a "contact filter" is generally applied to account for the finite size of the wheel/rail contact. As the contact between the wheel and the rail exists over an area, roughness with wavelengths that are short compared with the length of this contact patch are attenuated in their excitation of the system. Remington produced an analytical model for this contact filter [1] which requires an assumption to be made concerning the correlation between roughness across the contact zone (defined by a single parameter α).

More recently, a numerical 'Distributed Point Reacting Springs' model (DPRS), or 'mattress model', has been produced by Remington and Webb [2]. This replaces the contact by a set of independent non-linear springs. For a given roughness profile, the total force in the springs is evaluated to give a 'blocked force'. In order for the overall dependence of the contact force on the deflection to follow the correct non-linear relationship, each spring must have a force proportional to the square root of the local deflection. Moreover, the radii of curvature of the wheel and rail used in the calculation have to be adjusted in order for the contact area to be calculated correctly. Roughness data measured on many parallel lines is processed by this model, the result of which is a blocked force as a function of longitudinal position. If this is then divided by the nominal contact stiffness it yields an equivalent filtered roughness [3].

By using the DPRS model with several sets of measured roughness data and comparing the spectra of filtered and unfiltered roughness, the mean contact filter effect has been derived as a frequency domain result [3]. This is found to be similar to that obtained from the earlier analytical model [1] for wavelengths down to about 0.7 times the contact patch length, but at shorter wavelengths the DPRS model does not attenuate the roughness as much as the analytical model.

Often, however, measurements of roughness data are available only on a single line that is taken as typical of the running band. In such situations a frequency domain filter may be applied, such as the analytical model or the previous results from the DPRS model. However, where time-domain calculations of the response of the wheel/rail system are to be carried out, it is necessary to filter the roughness in the time domain. Such situations include the response to large amplitude roughness [4] and to discrete features on the wheel or rail, such as wheel flats [5] or rail joints [6]. While the DPRS model allows this, it is too complex, especially if only a single line of roughness data is available.

For these reasons, a two-dimensional 'mattress' model is investigated in the current report. As in the three-dimensional DPRS model, the Hertzian contact is replaced by a set of independent springs, but these are now located along a single line. Unlike the three-dimensional DPRS calculation, it is found in this case that the overall force / deflection relationship for the *three*-dimensional case is reproduced by this *two*-dimensional model if the springs are chosen to be linear. Nevertheless, as for the three-dimensional DPRS model, the radius of curvature of the wheel has to be adjusted in order to keep the correct contact patch length and static deflection for a given load. This model is described in Section 2. In Section 3 other existing contact filter models are described.

For assessing their three-dimensional version of the DPRS model, Remington and Webb [2] developed a Boussinesq analysis of the contact filter. This, although slow, provided a more comprehensive analysis for the purposes of comparison. A similar Boussinesq analysis is

implemented and used here to evaluate the 2-D mattress model over a range of contact configurations. This is described in Section 4 and comparisons are made between the Boussinesq analysis and the 2-D mattress model in Section 5 to 7. In Section 8 the mattress model is implemented as part of a time-domain model of wheel/rail interaction.

2 TWO-DIMENSIONAL MATTRESS MODEL

2.1 Hertzian model

Consider the Hertzian contact geometry in Figure 1(a). Local deformation of both the wheel and rail occurs, although for clarity the figure shows the deformation as present on the wheel. The contact patch length is $2a$ and the 'distance of approach' of the wheel to the rail is δ.

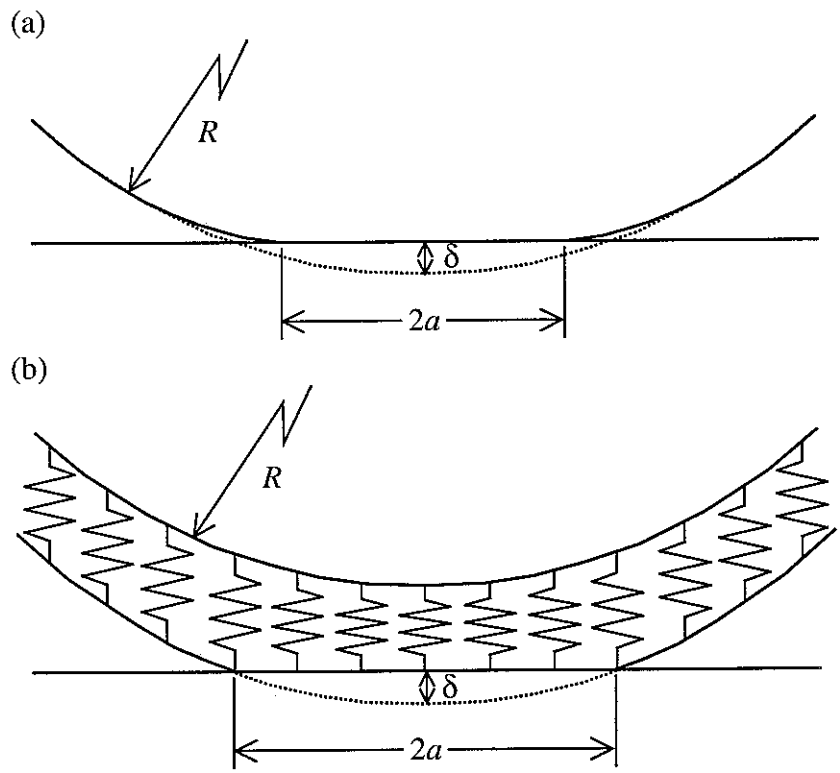

Figure 1. Contact between wheel and rail (a) Hertzian contact, (b) 'mattress' model. For simplicity only the wheel is shown to deflect.

Consider, for simplicity, the case in which the transverse curvature of the rail is the same as the radius of curvature of the wheel, R_w. Then the contact patch is circular and Hertzian contact theory [7] gives

$$a = \left(\frac{3 R_e P_0}{2E^*} \right)^{1/3} \tag{1}$$

and

$$\delta = \left(\frac{9 P_0^{\,2}}{4E^{*2} R_e} \right)^{1/3} \tag{2}$$

where P_0 is the total load acting at the contact, $E^* = E/(1-\nu^2)$ is the plane strain Young's modulus and R_e (= R_w for a circular contact patch) is an equivalent radius of curvature (NB the notation for both R_e and E^* differs from reference [7]; see also [8]). From the above it can be seen that

$$\delta = \frac{a^2}{R_e} \tag{3}$$

This is exactly true for a circular contact patch and approximately true for an elliptical contact patch. The pressure distribution is given by [7]

$$p(r) = p_0 \sqrt{1 - \left(\frac{r}{a}\right)^2} \quad r \le a \tag{4}$$

where r is the distance from the centre of the contact patch and p_0 is the maximum pressure (given by $P_0 = {}^2/_3\, p_0\, \pi a^2$ [7]). Note that deformation of the wheel (and rail, not shown) occurs over a greater length than $2a$ as the force at each location causes deformation over an area around that point. Equation (2) can be rearranged to give the contact force in terms of the static deflection

$$P_0 = c_H \delta^{3/2} \tag{5}$$

where c_H is the Hertzian constant, given by

$$c_H = \frac{2}{3} E^* R_e^{1/2} \tag{6}$$

2.2 Linearised Hertzian stiffness

Simple models of the contact require the linearised contact stiffness. This is obtained through a standard linearisation process. From equation (5),

$$k_H = \frac{dP_0}{d\delta} = \frac{3}{2} c_H \delta^{1/2} \tag{7}$$

Substituting for c_H from equation (6),

$$k_H = E^* R_e^{1/2} \delta^{1/2} \tag{8}$$

Also, from equation (3), $a = \sqrt{R_e \delta}$ giving

$$k_H = E^* a \tag{9}$$

where a is the radius of the contact patch under the given load and E^* is the plane strain Young's modulus defined above.

2.3 Two-dimensional discrete spring model

As an approximation for the contact, consider now a 'mattress' model of independent springs, shown in Figure 1(b). Here, the force at a given point only causes deformation at that point. Let the stiffness of these springs be k per unit length (the contact is here assumed to have a constant width rather than being elliptical). The equivalent radius of curvature of the wheel (to be determined) is R_m. The wheel surface is defined by

$$(R_m - y)^2 + x^2 = {R_m}^2 \quad => \quad y \approx \frac{x^2}{2R_m} \tag{10}$$

Hence the semi-length of the contact is given by substituting $x = a$ and $y = \delta$:

$$\delta \approx \frac{a^2}{2R_m} \quad \text{or} \quad a \approx \sqrt{2R_m \delta} \tag{11}$$

Note that this differs from the exact expression in equation (3) by a factor of 2, as noted in reference [7]. The total contact force is given by

$$P_0 = \int_{-a}^{a} f(x)dx, \text{ where } f(x) = \begin{cases} k(\delta - y(x)) & \text{if } \delta - y(x) > 0 \\ 0 & \text{if } \delta - y(x) \le 0 \end{cases} \tag{12}$$

Substituting for y and δ from equations (10, 11), this yields

$$P_0 = \int_{-a}^{a} k\left(\frac{a^2}{2R_m} - \frac{x^2}{2R_m}\right)dx = \frac{k}{2R_m}\int_{-a}^{a}\left(a^2 - x^2\right)dx = \frac{2ka^3}{3R_m} \tag{13}$$

The pressure distribution here is parabolic, rather than circular as given by equation (4). The two distributions are compared in Figure 2. In the left-hand figure they are compared for $R_m = R_w$ and equal maximum pressure. In the right-hand figure they are shown for an identical contact patch length and with the amplitude of the mattress model chosen to give the same integral over the length of the contact as the Hertzian model (the integral over the contact patch area would be strictly correct; however, the contact patch width is arbitrary in the mattress model).

Substituting for a from equation (11) in equation (13) gives

$$P_0 = \frac{2k}{3R_m}(2R_m\delta)^{3/2} = \frac{4\sqrt{2}\,k}{3}{R_m}^{1/2}\delta^{3/2} \tag{14}$$

However, the actual relationship between contact force and static deflection according to the Hertzian model is given by equation (5). Thus it can be seen that this can be replicated by choosing

$$k = \frac{3\,c_H}{4\sqrt{2}{R_m}^{1/2}} \tag{15}$$

i.e. the overall non-linear three-dimensional contact stiffness behaviour is reproduced correctly using a linear two-dimensional mattress model.

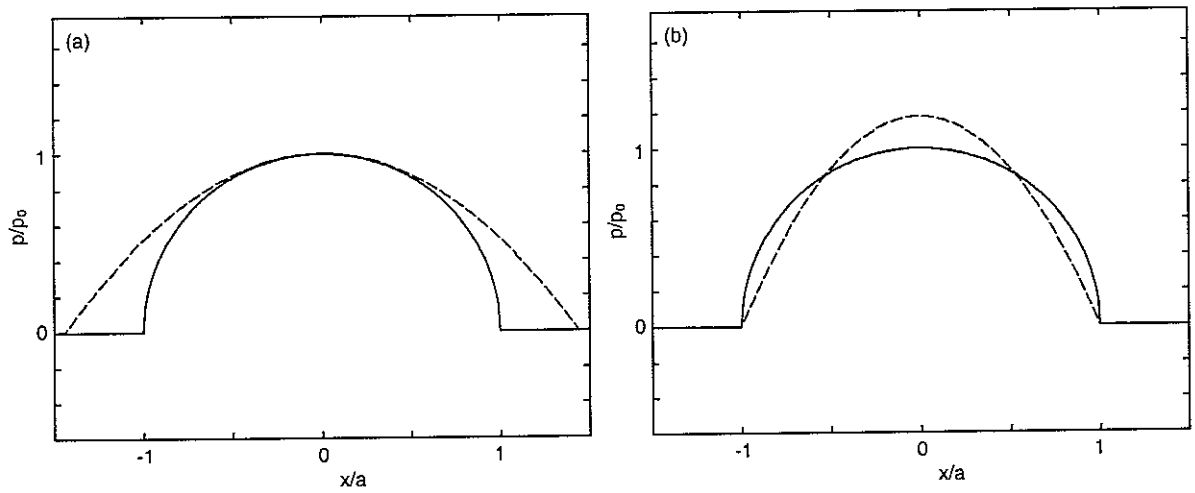

Figure 2. Pressure distribution from Hertzian model (solid line) and equivalent mattress model (dashed line). (a) for same radii and maximum pressure, (b) adjusted for same contact patch length and integral over length.

2.4 Adjustments to model

For noise predictions it is important that the contact patch has the correct length as this affects the wavelengths filtered, so adjustments have to be made. Ideally, it is desirable to have correct values simultaneously for:

- contact length,
- total contact load,
- deflection,
- wheel and rail geometry (radii of curvature).

Unfortunately these cannot all be satisfied simultaneously. Thus, comparing equations (3) and (11), it is seen that the mattress model does not give a correct contact patch length if the static deflection is correct. The best compromise is to adjust the wheel radius such that the other three quantities are correct and consistent. For the 2-D mattress model the adjusted wheel radius is

$$R_m = \tfrac{1}{2} R_e \tag{16}$$

where R_e is the equivalent radius of curvature for the original contact (for a circular contact patch it equals the wheel radius). Then equations (3) and (11) become consistent. Substituting this and equation (6) into equation (15), k reduces to

$$k = \frac{E^* R_e^{1/2}}{2\sqrt{2} R_m^{1/2}} = \tfrac{1}{2} E^* \tag{17}$$

The main difficulty with this adjustment is anticipated to be the case of two-point contact, for example at a rail joint, or where the curvature of the roughness is significant compared with

that of the wheel, for example at a wheel flat. In such situations the modified curvature of the wheel could yield misleading results.

2.5 Roughness processing

If the roughness profile (positive for an asperity) is given by $r(x)$, the total contact force when the wheel is centred at x is given by a modified form of equation (12)

$$P_0(x) = \int_{-a'}^{a'} f(x')dx', \text{ where } f(x') = \begin{cases} k(\delta - y(x') + r(x+x')) & \text{if } \delta - y(x') + r(x+x') > 0 \\ 0 & \text{if } \delta - y(x') + r(x+x') \le 0 \end{cases} \quad (18)$$

where the integration is performed over $-a' < x' < a'$, this range being extended to cover all potential points of contact. Thus, in order to process a set of roughness data, for each longitudinal position x the roughness in a region around x is chosen, $r(x+x')$ for $-a' < x' < a'$. This is combined with the circular profile of the wheel, $y(x')$, see equation (10), and a value of δ is sought such that the total force P_0 is equal to the nominal wheel load. The difference between this and nominal value of δ is stored as the 'equivalent roughness' at location x. Alternatively, the value δ could be imposed and the blocked force P_0 determined.

By comparing the spectra of the initial roughness and the equivalent roughness, a filter effect can be derived. In taking spectra of roughness signals, care must be taken to ensure that any overall trends are removed from the data so that discontinuities do not occur at the ends of the data block.

2.6 Results

Six sets of wheel roughness data are available and have been used in [3] to derive the filter effect of the DPRS model. These comprise three cast-iron block braked wheels, two sinter block braked wheels and one disc-braked wheel. The filter effect of the new two-dimensional (2D) mattress model has been derived from this same set of six wheels, and the average of all six has been formed. Whereas reference [3] used several parallel lines of roughness data, here only a single line is used corresponding to the centre of the contact. Results are shown in Figures 3 to 5 for a wheel load of 50 kN. The wheel radius is 0.46 m in each case. The value of c_H, the Hertzian constant, is determined using three different values of rail transverse radius of curvature: 0.23, 0.46 and 0.92 m. This affects the contact patch length, which has values of a = 5.92mm, 5.31 mm and 4.70 mm respectively. The dotted lines show the results for the six sets of wheel roughness and the thick solid line represents the average of these.

In each figure, results are also shown from the three-dimensional (3D) DPRS model. The results from the 2D mattress model are similar to those from the DPRS model for frequencies up to about 2.5 kHz (wavelengths down to about 11 mm). Above this frequency they are a few dB higher than the results from the 3D DPRS model.

Figure 6 shows the differences between the results of the 2D and 3D models. Although differences of up to 5 dB occur, the overall trends are well reproduced by this simple model. The average difference over all one-third octave bands is less than 2 dB.

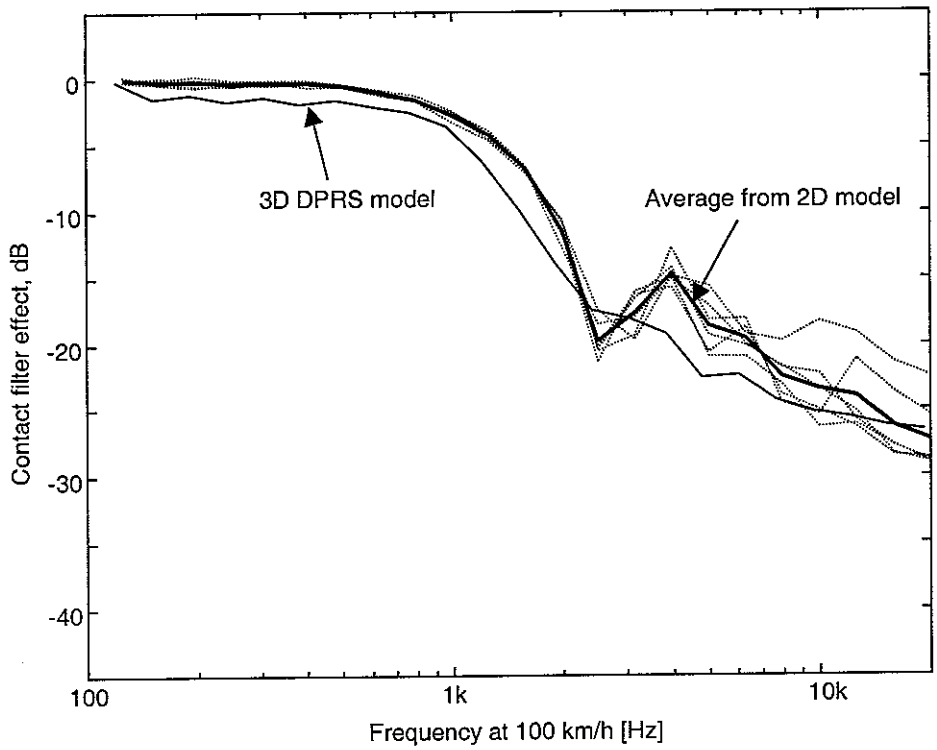

Figure 3. Contact filter effect for $R_w = 0.46$ m, $R_{rt} = 0.23$ m, $P_0 = 50$ kN.

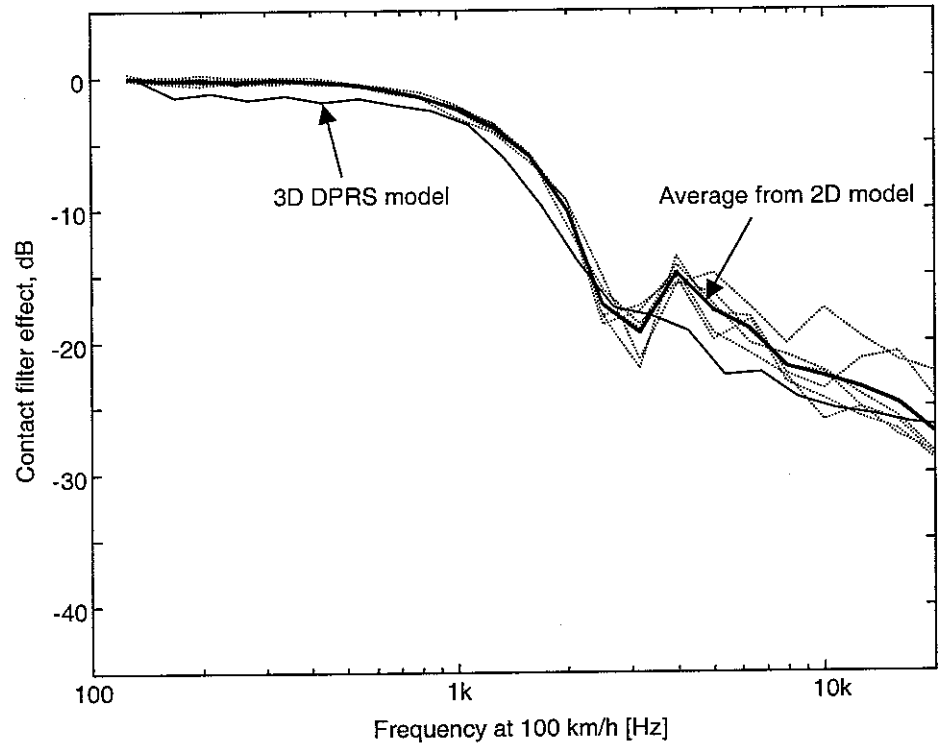

Figure 4. Contact filter effect for $R_w = 0.46$ m, $R_{rt} = 0.46$ m, $P_0 = 50$ kN.

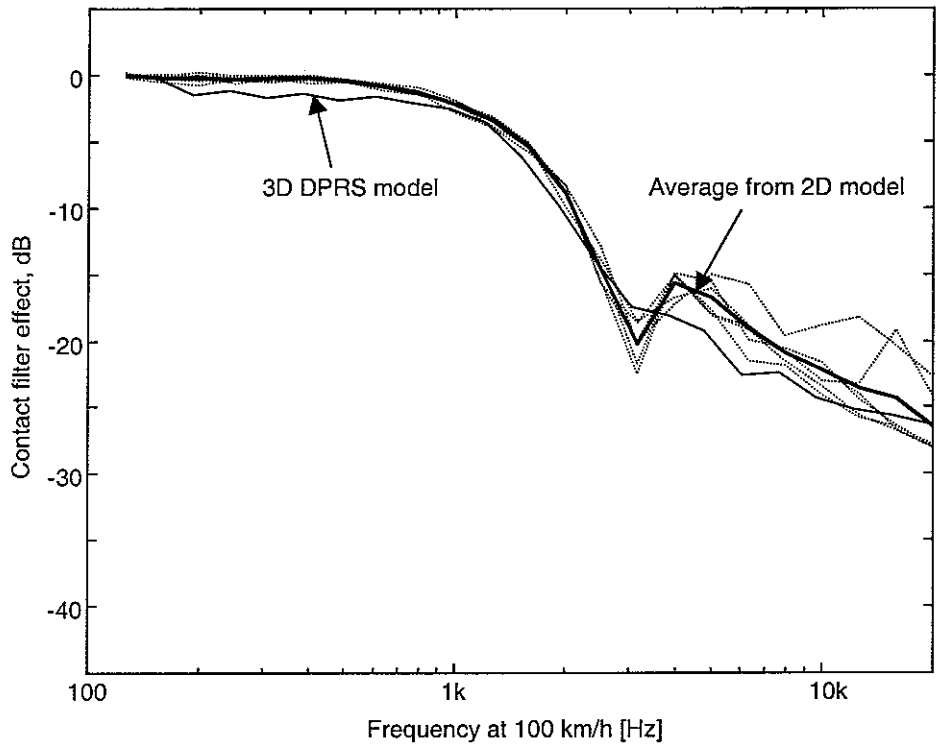

Figure 5. Contact filter effect for R_w = 0.46 m, R_{rt} = 0.92 m, P_0 = 50 kN.

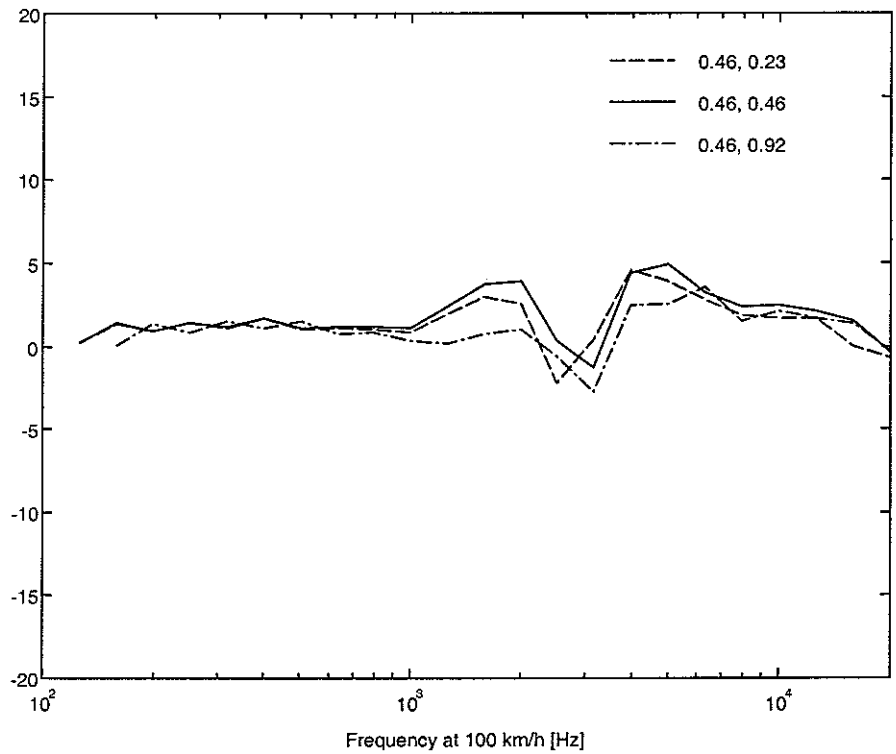

Figure 6. Difference in contact filter effect between 2D and 3D DPRS model for wheel radius 0.46 m and rail radii of curvature 0.23, 0.46 and 0.92 m.

3 OTHER MODELS OF THE CONTACT FILTER EFFECT

For comparison, three simpler models of contact behaviour have been studied.

3.1 Average deflection over the contact

As the simplest form of averaging for the contact, the average deflection was calculated over the nominal contact length. This is equivalent to convolving the input roughness with a rectangular window equal to the length of the contact. This provides an equivalent roughness, which can also be multiplied by the linearised stiffness to give the blocked force.

The filter effect of a rectangular window is well known (*e.g.* [9]), and for the quantities here is:

$$G(\lambda) = \frac{\sin(2\pi a/\lambda)}{2\pi a/\lambda} = \frac{\sin(\pi f_{ND})}{\pi f_{ND}} \tag{19}$$

where

λ wavelength,
a semi-length of contact patch,

and a dimensionless frequency has been defined as $f_{ND} = 2a/\lambda$.

The result from equation (19) is shown in Figure 7. Dips appear at $f_{ND} = 1, 2, 3, \ldots$. Although the graph shows the magnitude of equation (19), in fact the function changes sign at each minimum.

The rectangular window model is essentially a linear average across the contact length. Because the mattress model is based on a set of linear springs, it too is basically a linear average and under many conditions should provide very similar results. Differences between the window model and mattress model are:

- In the window model a constant averaging length is used whereas in the mattress model the length varies with the contact conditions.
- In the window model tensions are possible whereas in the mattress model contact is lost if tensions are predicted.

3.2 Analytical contact filter

An analytical expression for the contact filter was derived by Remington [1]. For a circular contact patch of radius a, the filter transfer function is given by

$$|H(k)|^2 = \frac{4}{\alpha}\frac{1}{(ka)^2}\int_0^{\tan^{-1}\alpha} J_1{}^2(ka\sec\psi)\,d\psi \tag{20}$$

where $k = 2\pi/\lambda$ is the roughness wavenumber, λ being the wavelength, and α is a parameter that describes the degree of correlation between roughness across the width of the contact

zone at a given wavenumber. Large values of α imply poor correlation. It is unclear from reference [1] what value of α should be used. $|H(k)|$ is the filter weighting applied to the roughness amplitude at wavenumber k.

The result of this model, $|H(k)|$, is shown in Figure 7 for a value of α of 0.1 (corresponding to high correlation across the contact width). It can be seen that the dips in the filter occur at values of f_{ND} that are greater than those from the rectangular window and that the filter has a greater attenuation at high frequencies than the rectangular window.

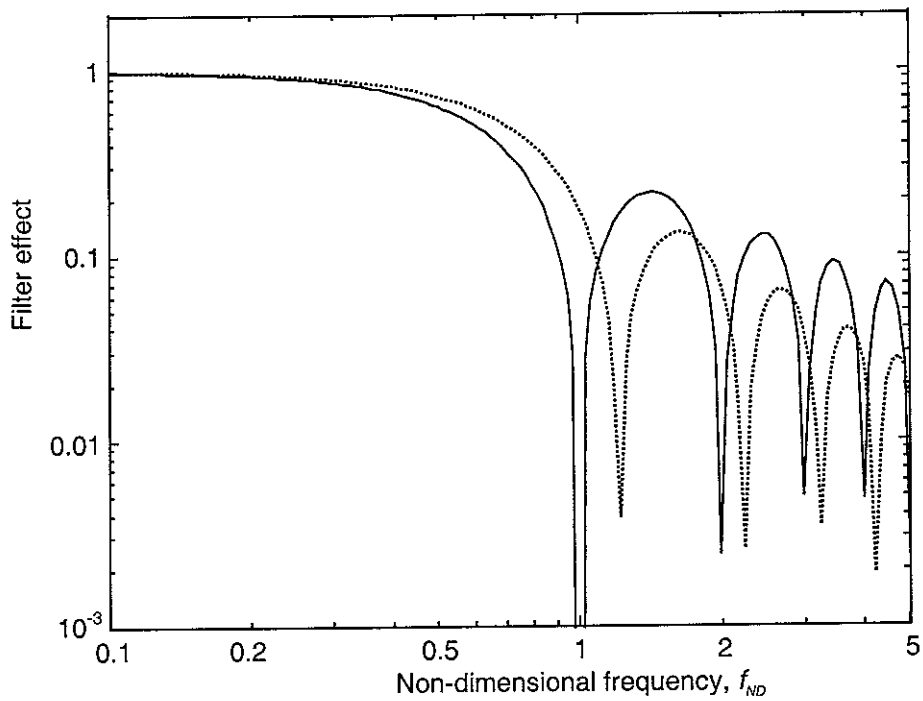

Figure 7. Contact filter effect for rectangular window (solid) and from Remington analytical model for α=0.1 (dotted).

3.3 Geometric filter

Although not a contact filter, another method of processing roughness data should be mentioned. Roughness profiles are usually measured with probes that have a small radius of curvature. Consequently, when the wheel/rail contact, with its larger radii of curvature, runs over this roughness, its geometry modifies the roughness seen by the system. This effect is purely due to the size of the wheel and rail, not due to static deflection of the contact spring. Thus it is equivalent to measuring the roughness with a probe of the same radius as the wheel itself. The geometric filter has a different effect on peaks and dips in the roughness.

The geometric filter is described in [10, 11]. If the roughness profile is given by $r(x)$, positive for an asperity, the 'filtered' roughness is given by

$$r_g(x) = \max_{-a' \le x' \le a'} \{r(x+x') - y(x')\} \tag{21}$$

where $y(x')$ is the circular profile of the wheel, see equation (10), and the range considered $-a' < x' < a'$ should be extended to cover all potential points of contact.

4 BOUSSINESQ ANALYSIS

4.1 Approach

Following the approach of Remington and Webb [2], the Boussinesq analysis has been programmed initially to give the "blocked force", *i.e.* the force assuming that distant points on the two contacting bodies maintain the same separation (*i.e.* the wheel does not follow the profile). This is simpler to implement than the alternative of calculating the deflection for a known force, although the latter enables an "equivalent roughness" to be generated that corresponds to a constant (quasi-static) wheel load. This has also been implemented (see below).

The analysis has been programmed in Matlab. Two variants of the program were initially produced. The first provided output for a single position on a single roughness feature. The second provided a spectrum for a cosine wave of various wavelengths. Later variants of each were produced to determine an equivalent roughness for a constant force. When coding the analysis of [2], careful attention to the detail in the paper was found to be necessary.

4.2 Principle

In Boussinesq analysis [2, 7] the deflection is specified around a point load on a uniform half-space, as shown in Figure 8.

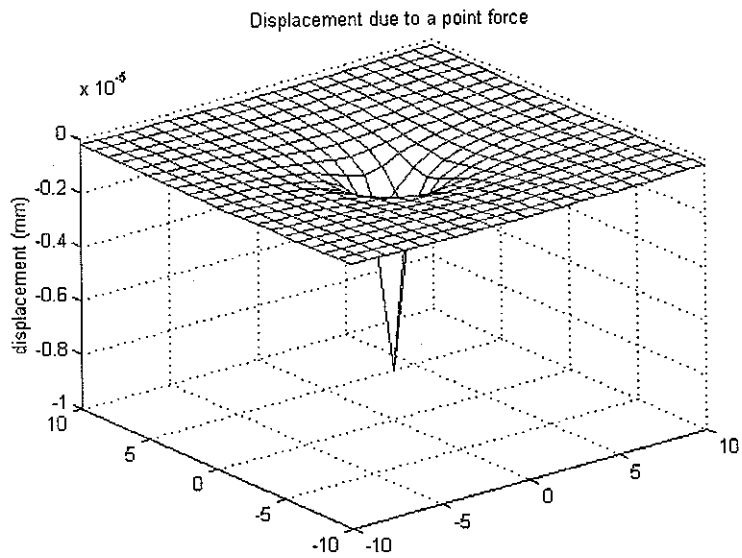

Figure 8. Boussinesq prediction of displacement around a concentrated load on a half-space.

To extend this analysis to a pair of contacting bodies, the contact zone is divided into a regular grid of points. A series of loads is considered at the nodes of the grid, and a corresponding set of displacements. If the load distribution at these points was known for the contact between the two bodies, using superposition the resultant displacement at any point could be found. Remington and Webb [2] show how this can be expressed in matrix terms, as

$$\{u\} = [A]\{P\} \tag{22}$$

where u is a vector of displacements at each node, P is a vector of forces at each node and A is a matrix described in [2] that implements the superposition process. The elements of A are [2]:

$$A_{ij} = \frac{2(1-\nu^2)}{\pi E\left\{(x_i - x_j)^2 + (y_i - y_j)^2\right\}^{1/2}} \qquad i \neq j \qquad (23a)$$

$$A_{ij} = \frac{2m(1-\nu^2)}{EA^{1/2}} \qquad i = j \qquad (23b)$$

where:

E	Young's modulus
ν	Poisson's ratio
x, y	co-ordinates of nodes
A	area of (square) element at each node
m	factor for displacement of a finite square area, given as 0.95 in [2].

In fact, the load at each point on the contacting bodies is not known. Instead the displacement is known, although only for points within the contact itself. Beyond the contact region the load is zero and the displacement is unkown. In this circumstance the problem becomes:

Given the displacements within the contact area

Find the loads within the contact area

To solve this problem equation (22) is applied to points within the contact area alone. However, the extent of the contact is not known *a priori*, so the following steps have to be repeated until the contact conditions are satisfied.

1. Estimate the boundaries of the contact area.
2. Assemble matrix A for points within the contact area.
3. Determine the vector of displacements within the contact (u) from a knowledge of the contact geometry.
4. Calculate the load distribution for that estimate by inverting equation (22).
5. Check for tensions (impossibility) and delete those points from the contact area.
6. Check for areas where surfaces intersect but have zero load (impossibility) and add these points to the contact zone.

Once the contact conditions are satisfied and the load distribution within the contact zone is determined, the displacements can be calculated outside the contact zone. Outside the contact zone the loads are zero, so a load distribution can now be assembled for whatever area is of interest. Once the A matrix has been assembled for the extended area, equation (22) can be used to calculate the required distribution of displacement.

For an analysis based on a constant load, an extra check is made on the total load and the height of the wheel is adjusted before the next iteration. The linear contact stiffness is used to

determine the extent of this adjustment. Once this has converged, the resulting contact deflection is used as a measure of the filtered roughness.

4.3 Implementation

The major stages in the basic analysis are:

1. gather input data,
2. set up a mesh to represent the analysis area,
3. determine the initial expected deflection at each node of the mesh,
4. assemble a vector of points where contact is expected,
5. implement the Boussinesq analysis based on these points,
6. determine if there are any tensions in the field of analysis, and if so delete these points,
7. repeat the analysis until there are no points with tensile forces,
8. check that this answer does not have points of contact outside the field of analysis (not yet implemented, although a scheme is available),
9. calculate and display the required data.

In the version implemented to date, the initial estimate of the contact area always overestimates the actual zone, so it has not been necessary to implement the check in point 8 above. Initially, the results were checked visually from 3-D plots to confirm this. One way to check for this automatically would be to ensure that wherever intersections of the two surfaces occurred there was a compressive load.

If a spectrum is required, the analysis is repeated for different wavelengths that give four equi-spaced subdivisions within each 1/3 octave band.

4.4 Running the programs

Data are input by directly editing the code. Some standard features such as cosinusoids are included for "commenting" out or in as required.

Input data required are:

- dimension of the side of the basic square of the mesh that makes up the analysis region,
- number of basic squares on each side of centreline,

- effective radius of curvature for x direction (equivalent spheroid on plane – equal to wheel radius),
- effective radius of curvature for y direction (equivalent spheroid on plane – combined effect of wheel transverse curvature and rail radius),

- Poisson's ratio,
- Young's modulus,

- basic deflection, *i.e.* the initial compression before the roughness is superposed (edit or comment in/out as required),
- matrix to specify roughness, *e.g.* sinusoidal (edit or comment in/out as required).

5 PRECISION OF THE BOUSSINESQ ANALYSIS

5.1 Contact of smooth surfaces

The precision of the Boussinesq analysis was investigated by comparing its predictions for the contact between a sphere and a smooth plane with the results of classical Hertzian analysis. This is equivalent to the case of a wheel on a rail, the transverse radius of which is equal to the wheel radius. In both cases a circular contact patch is obtained.

The basic geometry chosen for the comparison was:

- radius of the contacting bodies (equivalent sphere on plane) R_e = 500 mm,
- contact compression (δ) 40 μm and 60 μm.

The material properties chosen were:

- Young's modulus 210 GPa,
- Poisson's ratio 0.3.

A typical plot of contact stress is shown in Figure 9, which is for a mesh size of 0.5 mm and a compression of 60 μm. Tables 1 and 2 compare predictions for various mesh sizes. In all these results the Boussinesq analysis overestimates the load. Within this range the error is roughly proportional to the mesh size. Calculation time with the present code means that it is inconvenient to do a parametric analysis with a mesh size less than 0.5 mm.

Results are also given from the 2-D mattress model for comparison. For this model, the differences with the Hertz calculation are purely due to discretization errors and can be positive or negative.

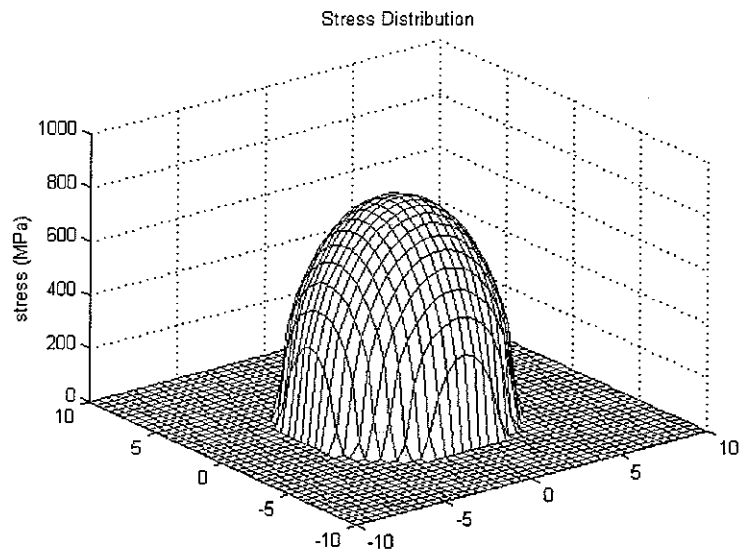

Figure 9. Boussinesq prediction of stress distribution at contact between a sphere and a plane surface; compression 60 μm.

Table 1. Contact with a plane surface, basic deflection 40 μm, corresponding Hertzian load 27,520 N.

Size of mesh (mm) (active points)	Total load, Boussinesq (N)	% difference from Hertz	Total load, mattress (N)	% difference from Hertz
1 (69)	28,419	3.26	27,692	0.44
0.5 (241)	27,946	1.54	27,462	-0.21
0.25	27,736	0.78	27,512	-0.03

Table 2. Contact with a plane surface, basic deflection 60 μm, corresponding Hertzian load 50,559 N.

Size of mesh (mm) (active points)	Total load, Boussinesq (N)	% difference from Hertz	Total load, mattress (N)	% difference from Hertz
1 (97)	51,941	2.73	50,769	0.42
0.5 (373)	51,204	1.28	50,481	-0.15
0.25 (1489)	50,882	0.64	50,546	-0.03

5.2 Strategy for comparisons with rough surfaces

The 'blocked' forces are calculated using the Boussinesq model for several "roughness" geometries, varying:

(1) initial deflection,
(2) location of the contact on the roughness feature,
(3) amplitude of the roughness feature.

The blocked force has been used for the investigation rather than equivalent roughness, because it is easiest to calculate with the present scheme. Although displacement under a constant load will usually be more relevant, blocked force will also give an indication of the filter behaviour.

The following roughness geometries were investigated, results of which are given in the next two sections:

1. Co-sinusoid (corrugations, *i.e.* 2-dimensional). These waves give insight into the filter effect at different wavelengths. They are fully correlated across the width of the contact.
2. Shape representing a "dipped rail" (2-dimensional).

For these, the basic contact properties were the same as in the previous section, i.e. the radius of the contacting bodies (equivalent sphere on plane) is R_e = 500 mm, the initial contact deflection (δ) is 40 μm or 60 μm and the material is defined by a Young's modulus 210 GPa and a Poisson's ratio of 0.3.

A mesh size of 0.5 mm has been used unless specified otherwise. From Section 5.1 it is seen that this is sufficient to give the blocked force results within about 1.5%, whereas a finer mesh leads to impractically long calculation times.

6 RESPONSE TO A COSINE WAVE

6.1 Basic behaviour of a sphere on a cosine roughness (corrugation)

6.1.1 Boussinesq analysis

Some example results of the Boussinesq predictions are given in Figure 10 for a wavelength of 13.4 mm and three different amplitudes. In each case, for ease of visualisation, the deformation is attributed wholly to the sphere (the wheel) while the lower surface is pictured here as rigid. The upper figures show the deformed situation when the sphere is at a trough in the roughness, while the lower figures show the situation at a peak. Figure 11 gives corresponding results for a constant amplitude and varying wavelength of roughness.

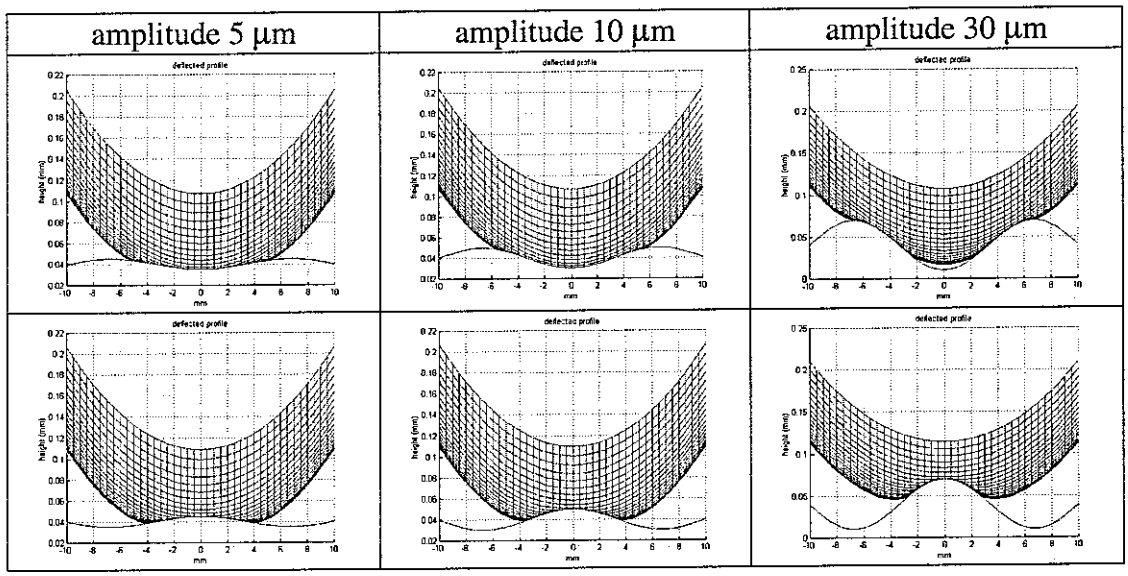

Figure 10. Deflected shapes from Boussinesq analysis for an initial compression of 40 μm and wavelength 13.4 mm.

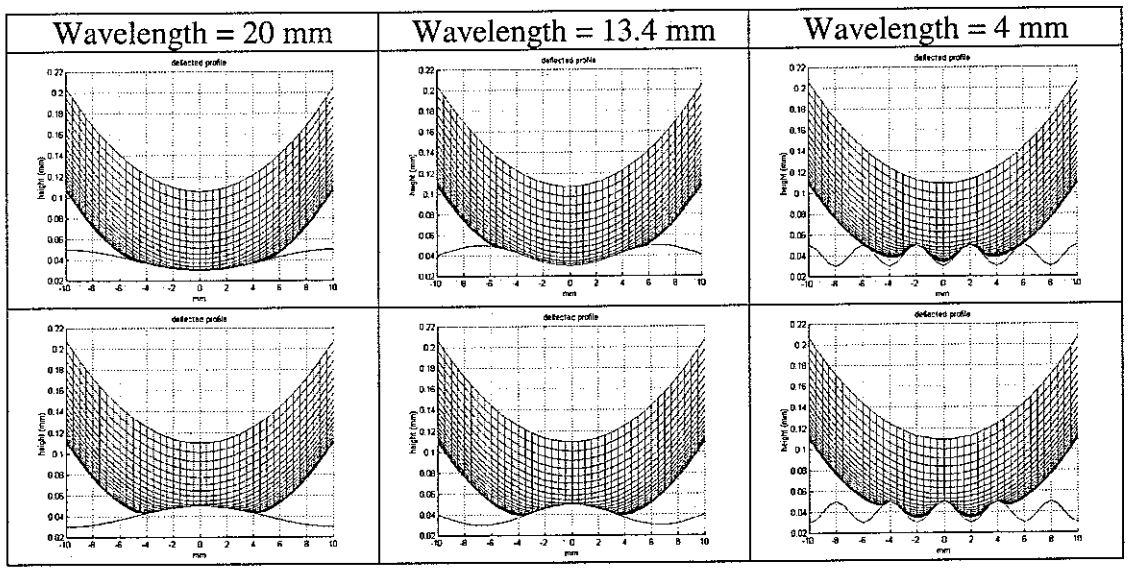

Figure 11. Deflected shapes from Boussinesq analysis for an initial compression of 40 μm and amplitude of 10 μm.

A characteristic of the Boussinesq results in Figures 10 and 11 is that, in both series, loss of contact occurs in the trough, in the first case at large amplitude and in the second case at short wavelength. In both cases the effect is related to the curvatures at the contact.

Figure 12 shows a selection of the stress distributions from the Boussinesq analysis corresponding to Figure 10. The separation of the contact into two at the trough of a large amplitude roughness can be seen in the top right picture.

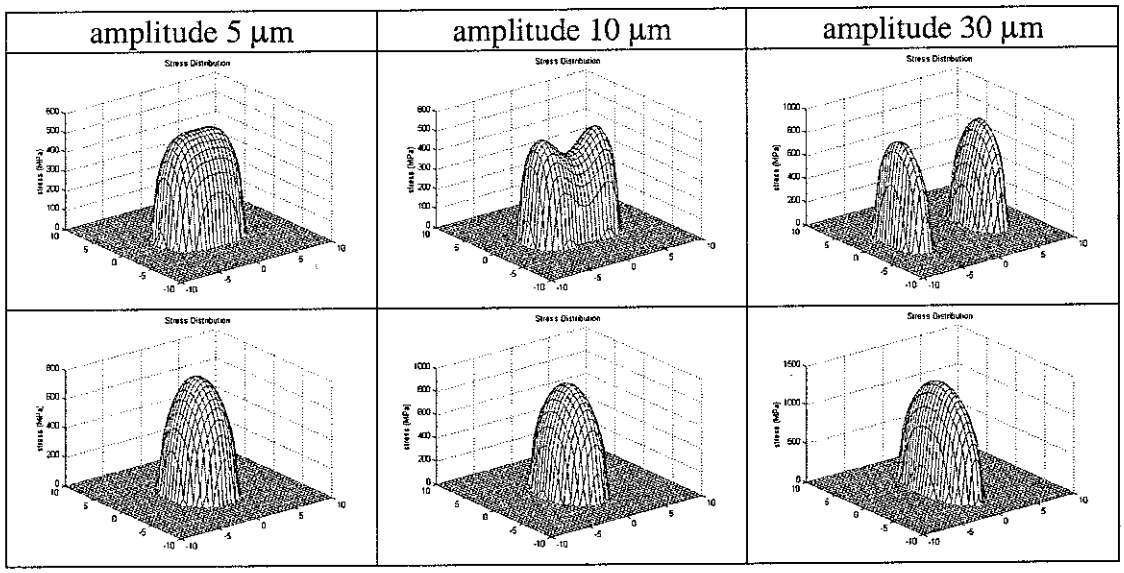

Figure 12. Stress distributions from Boussinesq analysis for an initial compression of 40 μm and wavelength 13.4 mm.

If the radius of curvature of the trough of the cosine wave is greater than the radius of the contacting sphere then initial contact is made at the bottom of the trough. However, if the reverse is true, then initial contact is made on the flanks of the cosine wave. Increasing the load complicates this simple behaviour, but the underlying feature remains.

The conditions for this transition can be calculated readily. The local curvature ($1/R$) of the trough of the sine wave is obtained from its second derivative with respect to distance:

$$\rho_r = h\left(\frac{2\pi}{\lambda}\right)^2 \tag{24}$$

where h is the amplitude of the cosine wave and λ is its wavelength. For the sphere (radius R_e) the curvature is:

$$\rho_s = \frac{1}{R_e} \tag{25}$$

The two will be equal when:

$$h = \frac{\lambda^2}{4\pi^2 R_e} \tag{26}$$

In Figure 10, the ratio ρ_s/ρ_r is 7.28, 3.64 and 1.21 and in Figure 11 it is 8.1, 3.64 and 0.32. This confirms that there are regions without contact at the trough for curvature ratios smaller than around 1; in the top right of Figure 10 this occurs for a ratio of 1.21.

Notice that because the mattress model uses an effective radius that is smaller than the actual one it will encounter this condition at a larger amplitude h.

6.1.2 Mattress model

The behaviour with the mattress model is similar to that with the Boussinesq model, but with the following differences:

1 An adjusted radius is incorporated (half size), so the radii of contact match at a larger amplitude of the wave, or a smaller wavelength.

2 In the mattress model it is assumed that points are in contact wherever the contacting surface is within the original outline of the cylinder that represents the wheel. As a result contact is not lost in the trough of a wave until the amplitude is greater than the initial compression, as shown in Figure 13.

From this analysis it seems that curvature of roughness features is an important quantity. This provides the motivation for using constant curvature within parametric studies, discussed in Section 6.3.

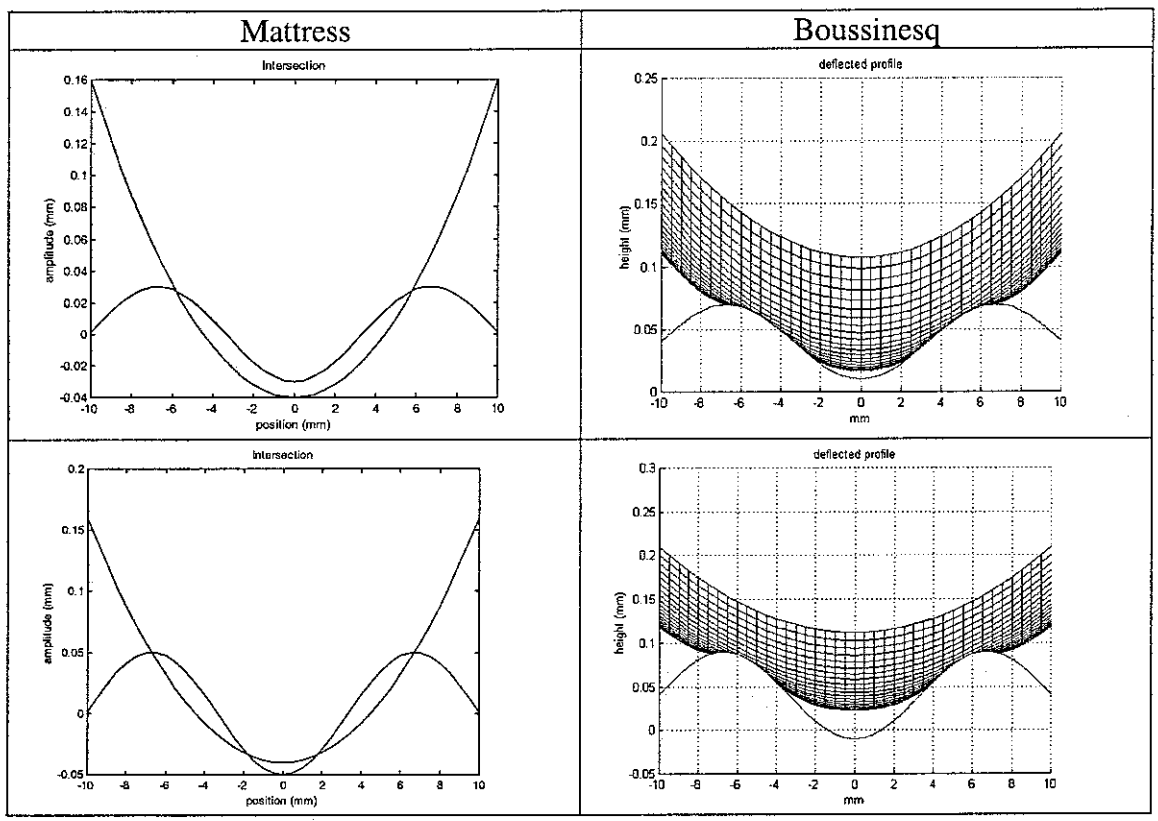

Figure 13. Deflected shapes from mattress model (left) Boussinesq analysis (right) for an initial compression of 40 μm and wavelength 13.4 mm. Top row: at amplitude 30 μm, mattress model maintains contact at trough, but Boussinesq does not. Bottom row: at amplitude 50 μm, both models lose contact at trough.

6.2 Parametric study of basic behaviour on a cosinusoidal roughness

In this section results are presented for two wavelengths (expressed as multiples of the contact patch semi-axis length a), a range of amplitudes of the cosine wave and different initial deflections. Two configurations are covered, as shown above, in which the contact is centred on the peak or the trough of the cosine wave.

Figure 14 shows the total load plotted against roughness amplitude for a nominal initial deflection of 40 μm. For each amplitude the upper results correspond to the load at a roughness peak and the lower results to that a trough. The wavelength is here $3a$, or 1.5 times the contact patch length.

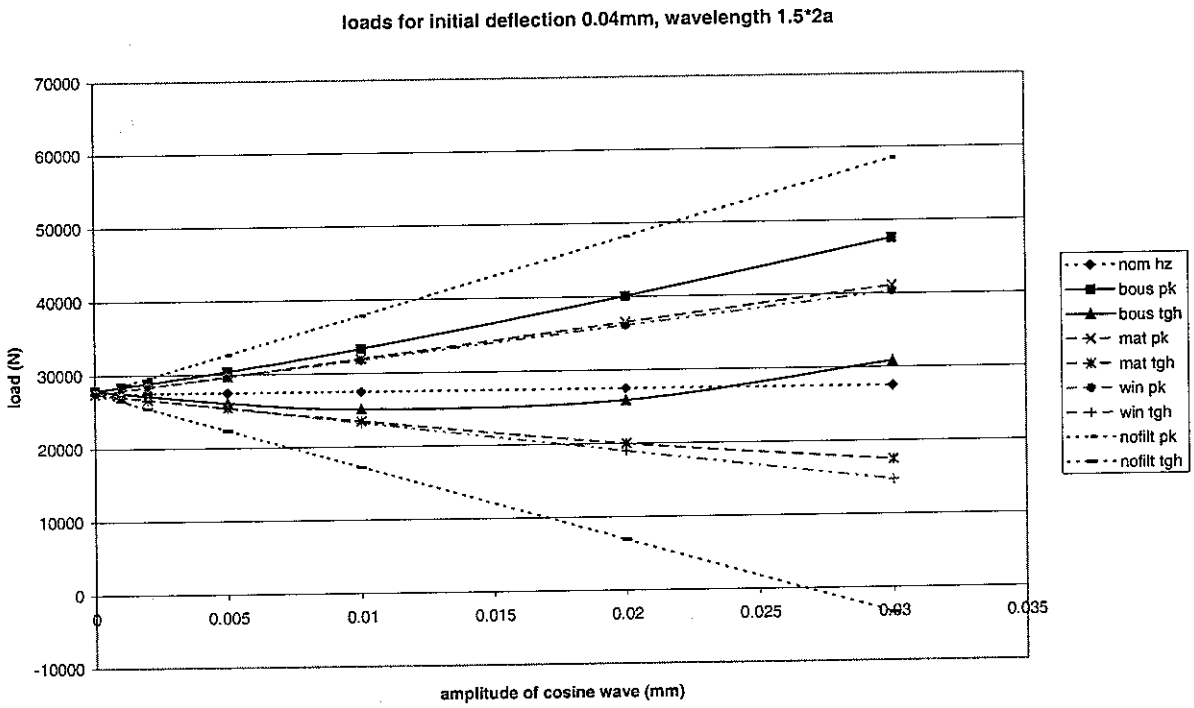

Figure 14. Load versus amplitude of cosine wave, initial deflection 40 μm, wavelength 1.5×contact length (2a), nom hz = contact with plane; pk = peak; tgh = trough; bous = Boussinesq; mat = mattress; win = rectangular window; nofilt = no filter (linearised Hertzian spring).

Predictions using the mattress model and the rectangular window (average) are quite similar even at large amplitudes of the cosinusoid. The results with no contact filter (based on a linear contact stiffness) show the largest variations in load, while the horizontal line corresponds to contact with a smooth plane.

The results for the Boussinesq analysis differ appreciably from the rest, even at amplitudes in the middle of the selected range. The most significant difference is when the contact is at the trough. This can be expected from Figure 10, because after a certain amplitude is reached, contact is lost in the trough, and the load is taken by the two neighbouring peaks. For amplitudes greater than 25 μm the load at the trough is greater than on a smooth plane.

To check that the 0.5 mm mesh was adequate for this comparison at large amplitudes a single point was recalculated using a 0.25 mm mesh for 30 μm amplitude with the wheel at the peak. The corresponding loads were 47,566 N for the 0.5 mm mesh and 47,146 N for the 0.25 mm mesh, from which it can be seen that the difference is small in this case (approximately 1%).

As explained in Section 6.1, when the amplitude $h = \lambda^2/(4\pi^2 R_e)$, the curvature of the roughness and the surface are equal at the contact. For the Boussinesq analysis of Figure 14, R_e = 500 mm and λ = 13.4 mm, which gives h = 9.12 μm. For the mattress model in Figure 14, the effective radius is 250 mm, which gives h = 18.2 μm (*i.e.* twice the amount). In both cases the curves at the trough appear to diverge from a straight line behaviour beyond these amplitude values. The divergence is more significant with the Boussinesq analysis as the body loses contact at lower wave amplitudes than the mattress model, as shown in Figure 13.

Loads at the peak are less affected, because in that configuration the roughness merely changes the curvature of a single point contact. With the Boussinesq analysis this change in geometry leads to an increasingly elliptical (shorter) contact patch, as shown in Figure 12, which might explain the divergence from the result for a rectangular window.

With the mattress model there is a much smaller increase from the linear trend of the rectangular window. Because it is two-dimensional the considerations of ellipticity of the contact described above do not apply. That there was an increase at all was at first less easy to explain. The increasing curvature of the roughness reduces the contact length, which might have been expected to reduce the load for a given compression compared with the windowed calculation. However, areas within the window that are outside the new contact length defined by the mattress model include the areas of negative displacements (tensions) shown in Figure 15, and because the mattress model eliminates these tensions it gives the higher loads seen in Figure 14.

Some results for a wavelength that is ¾ of the contact length are listed in Table 3 for an amplitude of 20 μm. Here it is found that a reversal of load occurs with the Boussinesq model, such that when the contact is centred on the trough the load is higher than when it is centred on the peak. The loaded geometry is shown in Figure 16 for contact centred at the trough. A similar effect is found with averaged and mattress models.

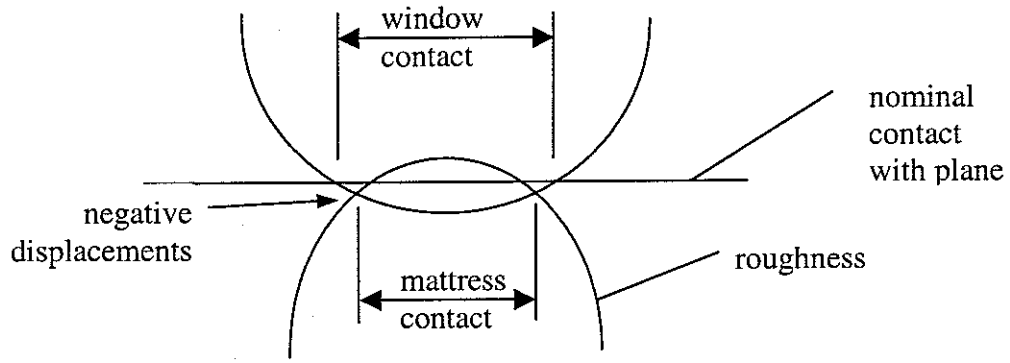

Figure 15. Diagram showing negative displacements within window.

Table 3. Loads with wavelength ¾ of contact length at 20 μm amplitude.

	load at peak (N)	load at trough (N)	difference (N)
Boussinesq	34,410	39,016	−4,606
Mattress (2D)	25,234	32,205	−6,971
Rectangular window (see Section 4.2)	23,254	31,788	−8,534
Linearised spring (see Section 4.1)	48,161	6,880	41,281

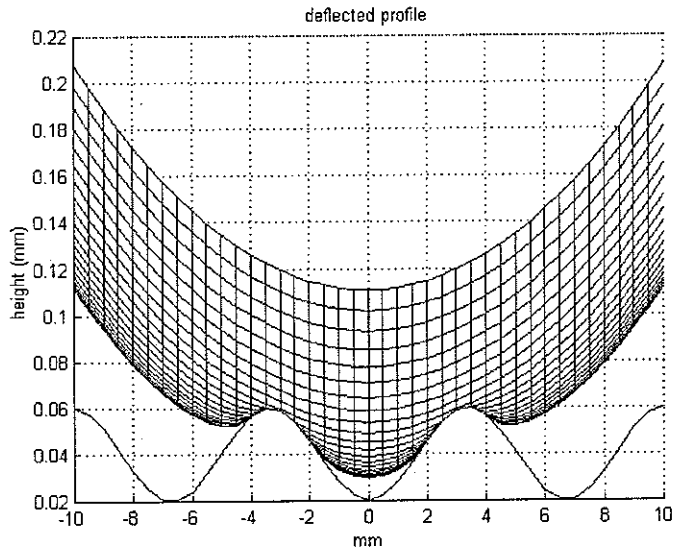

Figure 16. Deflected shape from Boussinesq analysis for wavelength ¾ of contact length

6.3 Filter effect as function of wavelength

In the previous section results were presented at two wavelengths. For analysing the production of railway noise the filter effect is required as a function of frequency. To generate curves of this kind using the Boussinesq analysis, the code used above was built into an iteration loop that produces load versus dimensionless spatial frequency of the cosine roughness wave. Dimensionless spatial frequency has been defined as $f_{ND} = 2a/\lambda$ (Section 3.1). The value $f_{ND} = 1$ signifies a wavelength equal to the contact patch length and corresponds to the first dip in the window function of equation (19), see Figure 7.

The filter effect has been determined for the Boussinesq and mattress models by taking the difference between the calculated loads at the peak and trough and dividing by the difference in the corresponding loads from the Hertzian calculation for a long wave (actually a plane surface at the appropriate total compression).

Two options to determine the amplitude of the cosine function used have been explored:

1. Constant curvature: in this case the amplitude is varied with wavelength according to equation (24) to keep curvature constant (expressed as the ratio of the radius of curvature of the roughness at the trough to the radius of curvature of the sphere).

2. Constant amplitude: in this case the amplitude is held constant (expressed as an amplitude ratio, amplitude of wave to nominal compression of contact).

The corresponding amplitudes used are shown in Figure 17. For the cases of constant curvature, the amplitude is inversely proportional to the square of the wavelength. At very long wavelengths the amplitude is therefore larger than the nominal contact spring deflection δ and loss of contact can occur at the trough. These cases are therefore not used for amplitudes greater than about half the nominal deflection δ. Actual roughness amplitudes (per one-third octave band) are generally around 10 μm at low frequencies and 0.1 μm at high frequencies, *i.e.* approximately between amplitudes defined by the curvature ratios of 10 and 1.

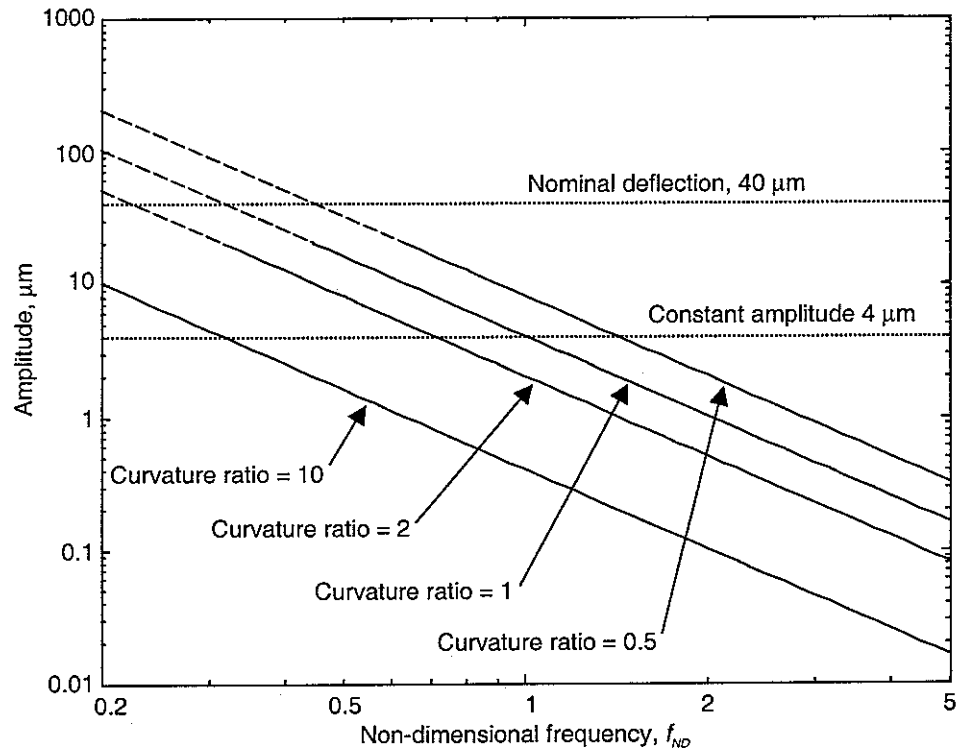

Figure 17. Amplitudes of cosine inputs used for evaluating Boussinesq and mattress models.

The results of the Boussinesq analysis are shown in Figure 18, calculated using a 0.5 mm mesh size and a nominal deflection of 40 μm. Results are shown for four different amplitudes of roughness defined by the curvature ratio. The filter effect can be seen to have a strong dip at f_{ND} = 1, 2, 3, ..., as in Figure 7 for the rectangular window. The filter characteristic also changes sign at each of these dips (not shown). The results vary only slightly with amplitude in the range used here. Even for the curvature ratio of 0.5 where, at the trough, the contact is on the flanks of the roughness and not in the trough itself, the filter effect is not significantly different from the results shown for lower amplitudes.

Figure 19 shows results for a constant amplitude of 4 μm as well as the previous results for a constant curvature ratio of 10. At high frequencies the constant amplitude experiences a larger filter effect as the contact cannot reach the bottom of the roughness profile (see Figure 11, right-hand picture).

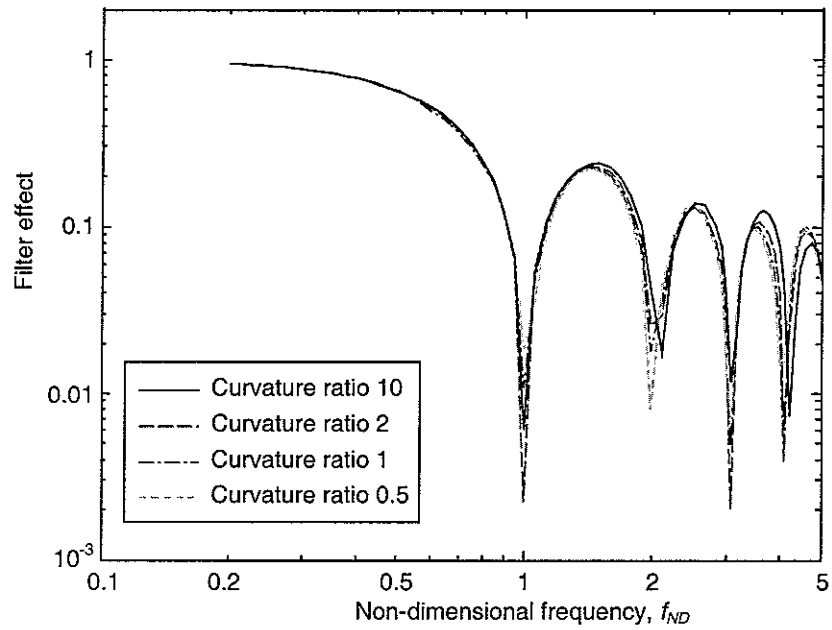

Figure 18. Contact filter effect for Boussinesq analysis, nominal deflection 40 μm, constant curvature ratio.

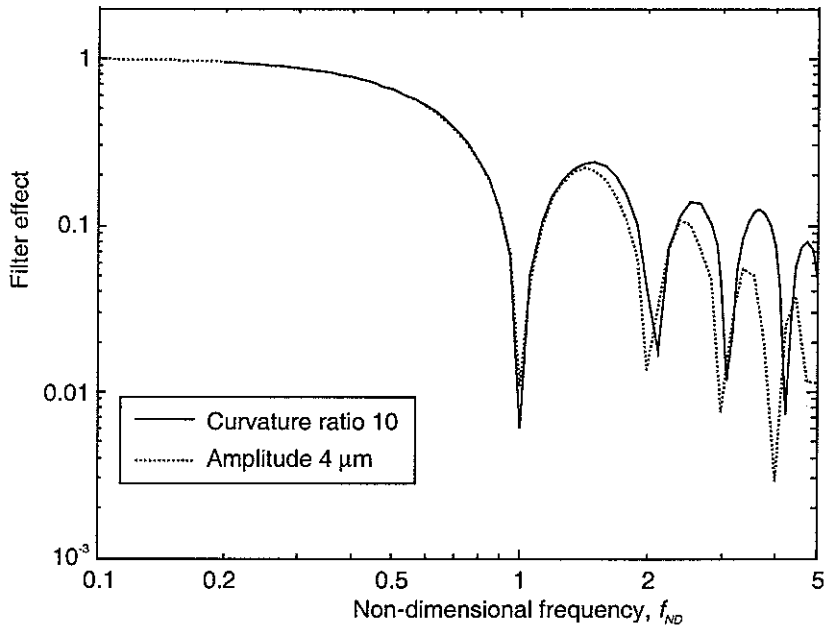

Figure 19. Contact filter effect for Boussinesq analysis, nominal deflection 40 μm: constant curvature ratio 10 and constant amplitude 4 μm.

In Figure 20 the results of the Boussinesq analysis are compared for two different nominal deflections, 40 μm as used above and 60 μm. The roughness amplitude is defined by a constant curvature ratio of 10, so that different amplitudes are used in the two cases. The results agree closely, although some differences can be noted at higher frequencies. Since the higher initial deflection causes a longer contact patch, discretization errors are likely to be smaller in this case; it is probable that the results for the lower deflection have been affected by this. This is probably the reason that the 60 μm results have a smoother trend at the peaks than the 40 μm results.

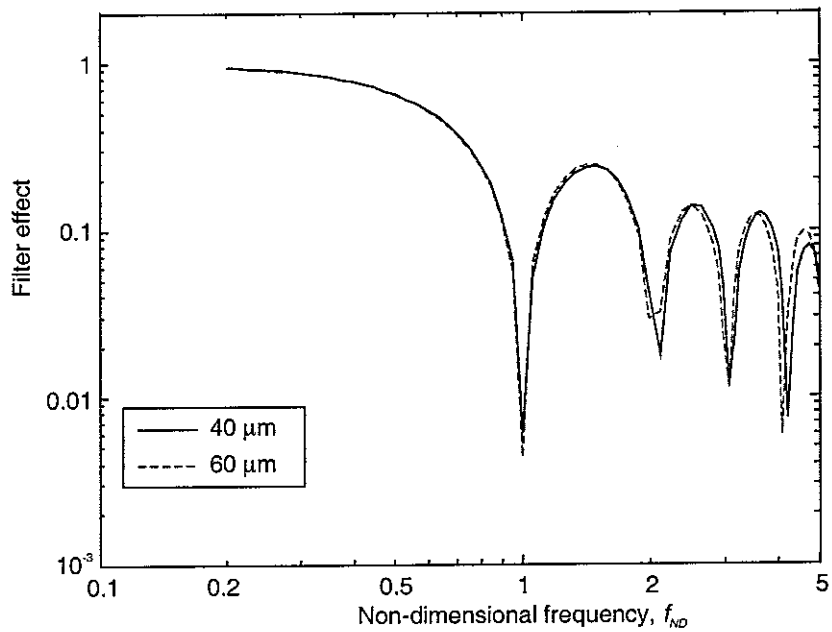

Figure 20. Contact filter effect for Boussinesq analysis with constant curvature, curvature ratio 10 for nominal deflection 40 µm and 60 µm.

Figure 21 shows the filter effect estimated using the two-dimensional mattress model for roughness amplitudes defined by a constant curvature ratio. Although some slight differences occur in the position of the first few dips for larger amplitudes, the curves converge at high frequencies to a result that is independent of amplitude. Note that the sign of the filter effect changes at each dip in the same way as for the rectangular window and Boussinesq analysis.

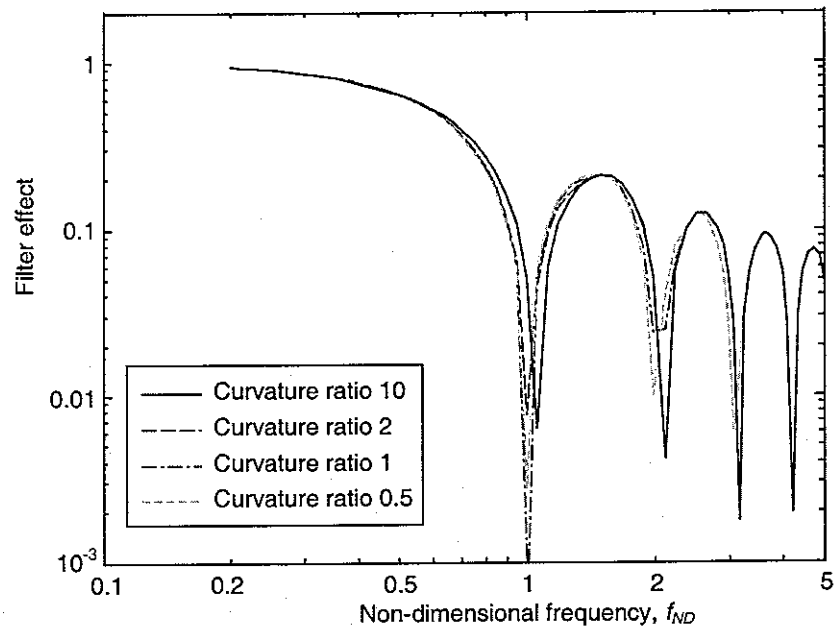

Figure 21. Contact filter effect for 2D mattress model, nominal deflection 40 µm: constant curvature ratio.

In Figure 22 the results of the Boussinesq analysis, two-dimensional mattress model and rectangular window are compared for an amplitude based on a curvature ratio of 10. Generally good agreement is seen between all three models, although with detail differences.

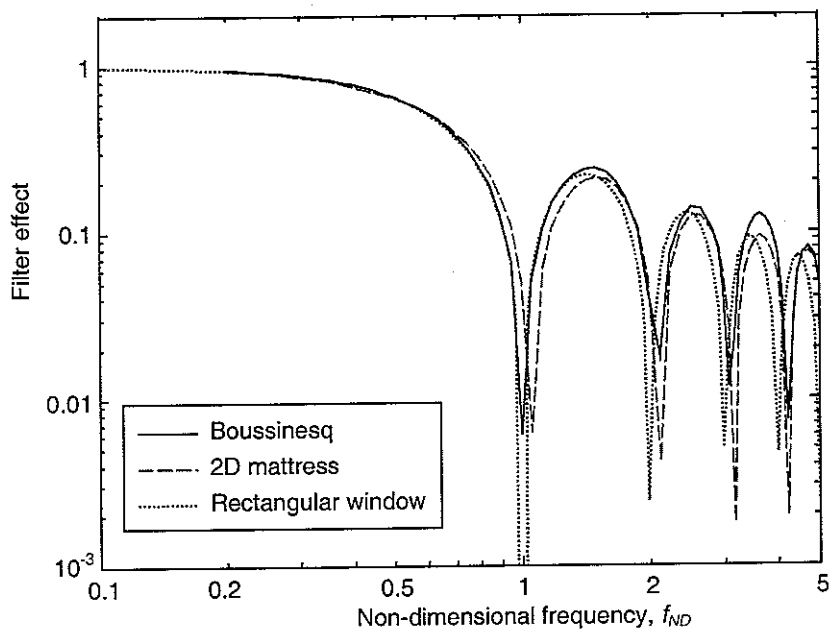

Figure 22. Contact filter effect for constant curvature, curvature ratio 10 from Boussinesq, mattress and rectangular window models.

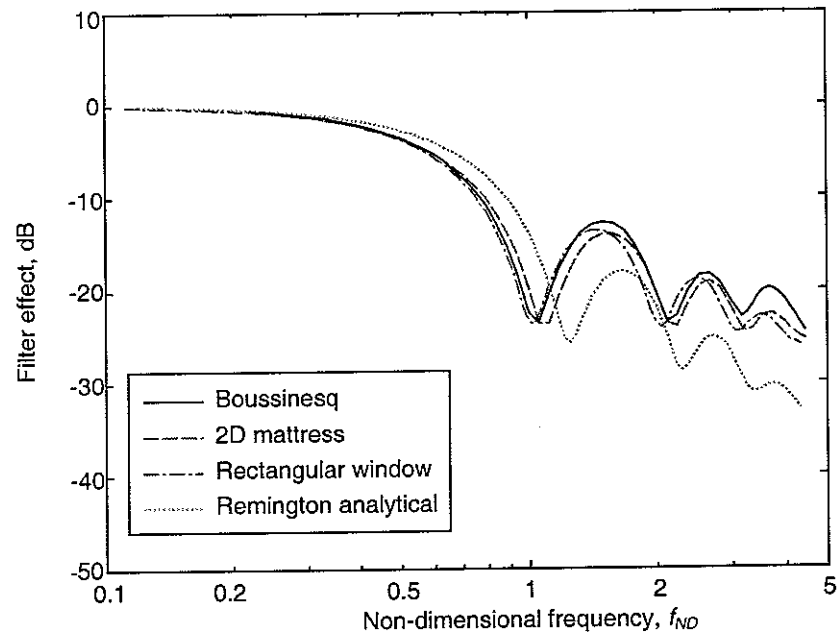

Figure 23. Contact filter effect for constant curvature, curvature ratio 10 from Boussinesq, mattress and rectangular window models, smoothed into one-third octave bands.

Since roughness is usually presented in one-third octave spectra, these results have been smoothed by averaging the results at four consecutive frequencies to form one-third octave band results in the form of a moving average. This is shown in Figure 23.

The difference between the various models and the Boussinesq analysis is shown in Figure 24 from which it is clear that the mattress model gives results that are within 3 dB of those of the more exact Boussinesq analysis. The differences around $f_{ND} = 1$ are attributable to a slight difference in the location of the first spectral dip. The differences at high frequencies may be partly due to effects of the mesh size (see Figure 20). Even the simple rectangular window

gives results that are within 4 dB of those of the Boussinesq analysis. The Remington analytical model, however, deviates from it by up to 10 dB in the frequency range considered.

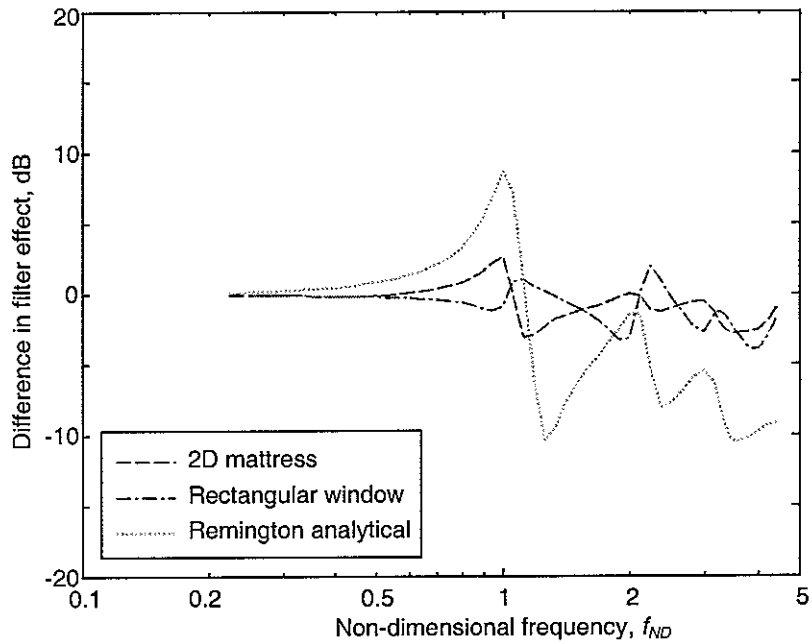

Figure 24. Difference in contact filter effect from mattress model, rectangular window and Remington analytical model compared with Boussinesq model for constant curvature ratio 10, smoothed into one-third octave bands.

In all the results of this section the contact deflection has been preset and the total contact force has been obtained. However, it is also possible to calculate the contact filter effect by ensuring that a particular total load is obtained and finding the contact deflection required. Figure 25 shows results that are calculated on this basis for a roughness amplitude determined from a curvature ratio of 10 and for preloads of 27.5, 30 and 50 kN.

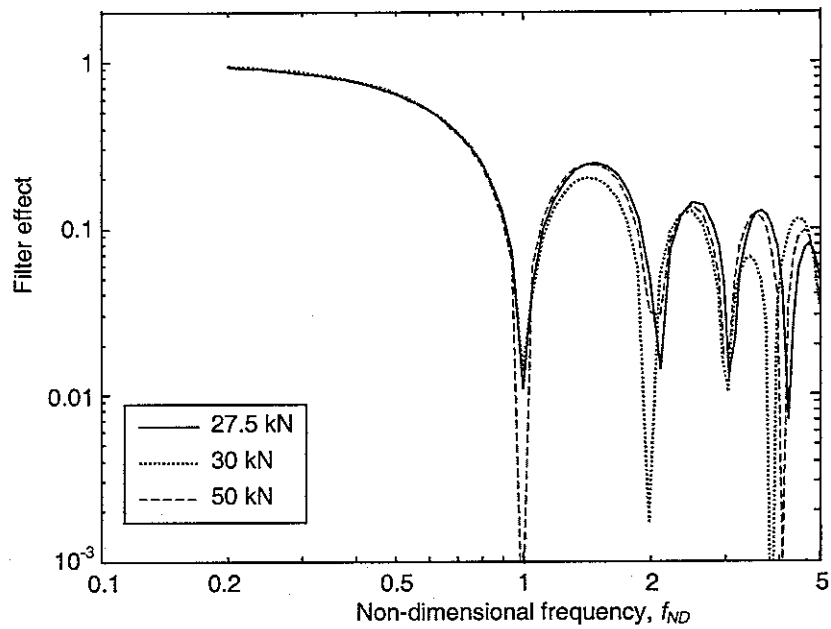

Figure 25. Contact filter effect for Boussinesq analysis with constant curvature, curvature ratio 10 for preload 27.5, 30 and 50 kN.

For the deflections of 40 μm and 60 μm considered previously the nominal preloads are 27.5 and 50.6 kN (see Table 1). The results for 27.5 and 50 kN are very close to those in Figure 20 for a constant deflection. This suggests that the contact filter results obtained from the blocked force and from the equivalent roughness are equivalent, at least for moderate amplitudes. However, it can be seen that the results for 30 kN differ considerably from those for 27.5 kN. This confirms that discretization errors are likely to be the cause of the different heights of the peaks at high frequencies.

7 RESPONSE TO A "DIPPED RAIL"

7.1 Background

Joints in continuously welded rails that are made in the field can result in a cusp-like discontinuity, typically of the form represented in Figure 26. This curve has been constructed from two intersecting quadratic curves [6], each with a length of l = 500 mm and a depth at the intersection of h = 3 mm. The equation for this shape is:

$$r(x) = 2h\left(\frac{|x|}{l}\right) - h\left(\frac{x}{l}\right)^2 \tag{27}$$

which is arranged to give $r(0) = 0$, $r(\pm l) = h$.

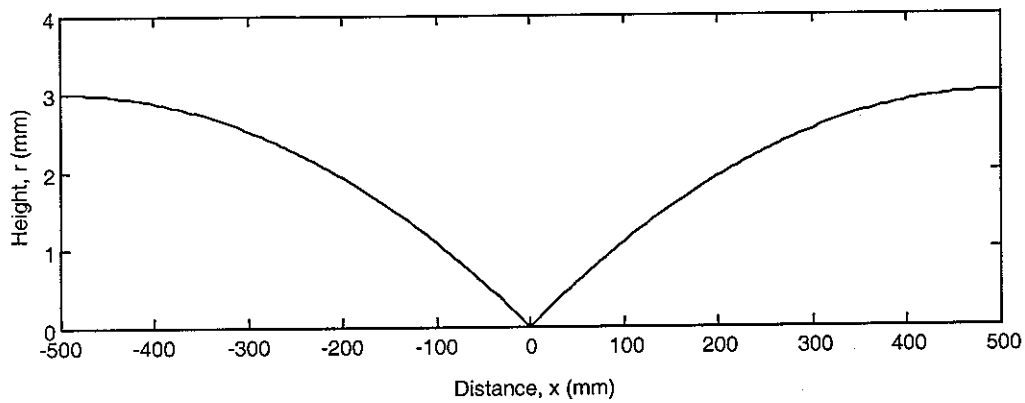

Figure 26 Idealised representation of dipped rail shape, height 3 mm, overall length 1 m.

7.2 Geometrical considerations

At first sight it appears that the adjusted radius (half size) of the 2-D mattress model would lead to gross differences when it encountered a discrete event such as a dipped rail, because it would go further towards the point of the cusp. Geometrical considerations, however, suggest that this might not be as significant as at first supposed.

Consider two spheres about to roll into a cusp as shown in Figure 27. These two spheres represent the actual wheel and the half-size wheel of the mattress model. Due to the size of the wheel, it cannot follow the complete roughness profile, even if the deflection of the contact spring is ignored. The effect of this geometric filter (see Section 3.3) depends on the wheel radius. For a dipped rail this effect can be obtained analytically, as described in Appendix A.

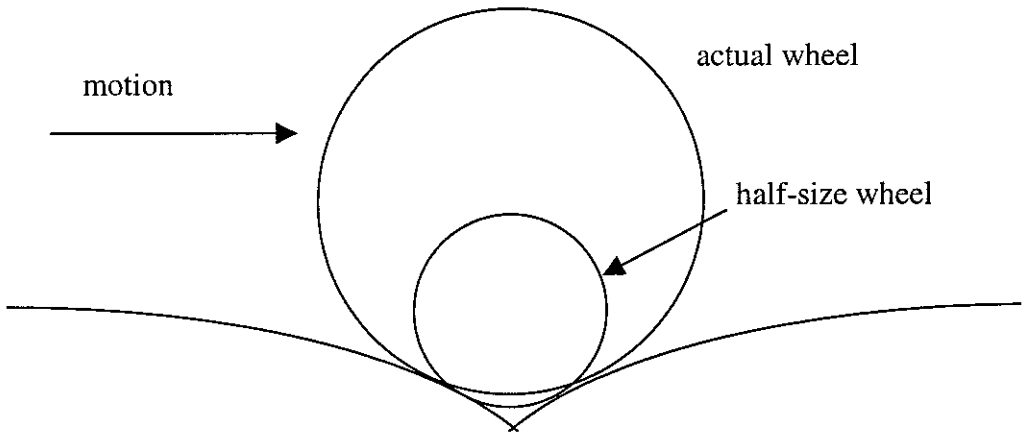

Figure 27 Wheels on a cusp.

The result is a quadratic function similar to equation (27), but with a depth that is reduced by a factor $\frac{l^2}{l^2+2R_w h}$ (the minimum height becomes $\frac{2R_w h}{l^2+2R_w h}$ instead of 0). The angle at $x = 0$ is reduced by an identical factor[1]. This factor is listed in Table 4 as a percentage for various values of wheel radius and for the typical conditions $h = 3$ mm and $l = 500$ mm used above. The difference in the depth of the dip and the slope at the cusp between the nominal wheel and the half-size wheel is only 0.6%. Therefore, for this typical configuration, the difference in excitation around the point of the cusp would be negligible.

Table 4 Percentage difference in the depth of the dip and in the slope at the cusp for $h = 3$ mm and $l = 500$ mm ($h/l = 0.006$).

R (mm)	l/R	difference from rail profile (mm)	% difference from rail profile	
8000	0.0625	0.48	16.1	
4000	0.125	0.26	8.76	
2000	0.25	0.14	4.58	
1000	0.5	0.070	2.34	
500	**1**	**0.036**	**1.19**	**nominal**
250	**2**	**0.018**	**0.60**	**half-size**
125	4	0.0090	0.30	
62.5	8	0.0045	0.15	
31.25	16	0.0022	0.075	

7.3 Effects of deflection

In this section the Boussinesq and 2-D mattress models are used to demonstrate the significance of local deflections on the geometrical analysis given above. Sample deflected shapes are shown in Figures 28 and 29.

Figure 28 compares predictions for the two models at a wheel centre position 1 mm from the cusp and for a deflection that is almost large enough to cause contact to the right of the

[1] The angle (change in slope) at the cusp is often used as a measure of the severity of a dip; for the quadratic function of equation (27) it is given by $2\phi = 4h/l$.

discontinuity as well as to the left of it. For the mattress model, any region where the curve is below the line of the cusp represents compressive forces. Because the mattress model is based on a smaller radius, the contact region occurs lower down the cusp and the corresponding height of the wheel above the datum is lower than for the Boussinesq model (a height of 0 – the datum – is defined as when the *undeformed* wheel could just rest at the height of the point of the cusp). This difference (actually 18 μm for the same load conditions) has already been seen in Table 4.

mattress model: height *above* datum 10 μm	Boussinesq model: height *above* datum 25 μm
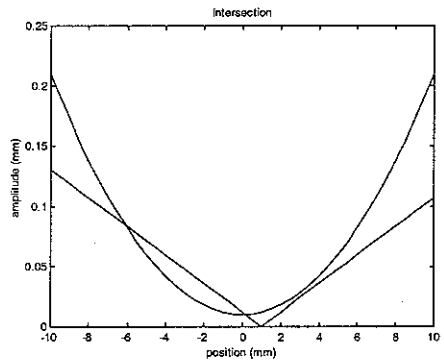	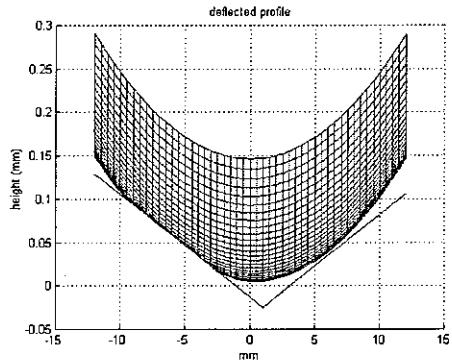

Figure 28 Deflected shapes for wheels on a cusp at last single point contact. The corresponding loads are approximately 10 and 12 kN respectively.

Figure 29 compares the two deflected shapes at a typical load, approximately 50 kN. Again, for the mattress model, any region where the curve is below the line of the cusp represents compressive forces. In this case with the mattress model contact occurs over the whole of the cusp, whereas for the Boussinesq model this does not occur. As with Figure 28, the mattress model again has dropped further into the dip, in fact by a similar amount.

mattress model: height *below* datum 20 μm	Boussinesq model: height *below* datum 5 μm
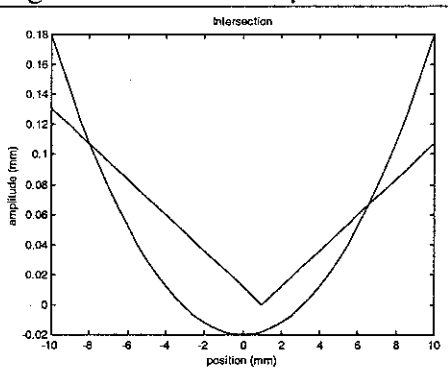	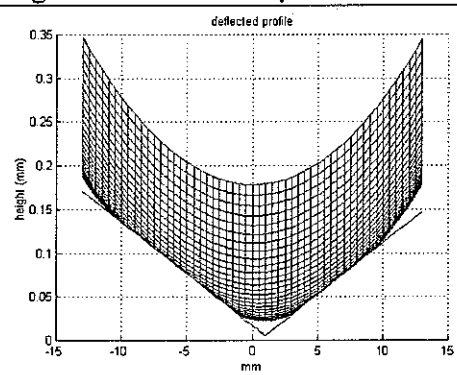

Figure 29 Deflected shapes for wheels on a cusp at typical load (approximately 50 and 48 kN respectively).

To see the load-deflection behaviour, results such as those in Figure 29 have been obtained for a range of compressions, and the total load calculated for each. Results are shown in Figure 30 for the wheel centred above the point of the cusp. It can be seen that the two curves are similar apart from a horizontal offset. Note that the deflection at zero load is equal to the height of the geometrically filtered profiles noted in the previous section. Thus, for the wheel

above the point of the cusp, the actual wheel is at 36 μm above the datum and the reduced size wheel is at 18 μm above the datum. These correspond to negative values ('compressions') in Figure 30.

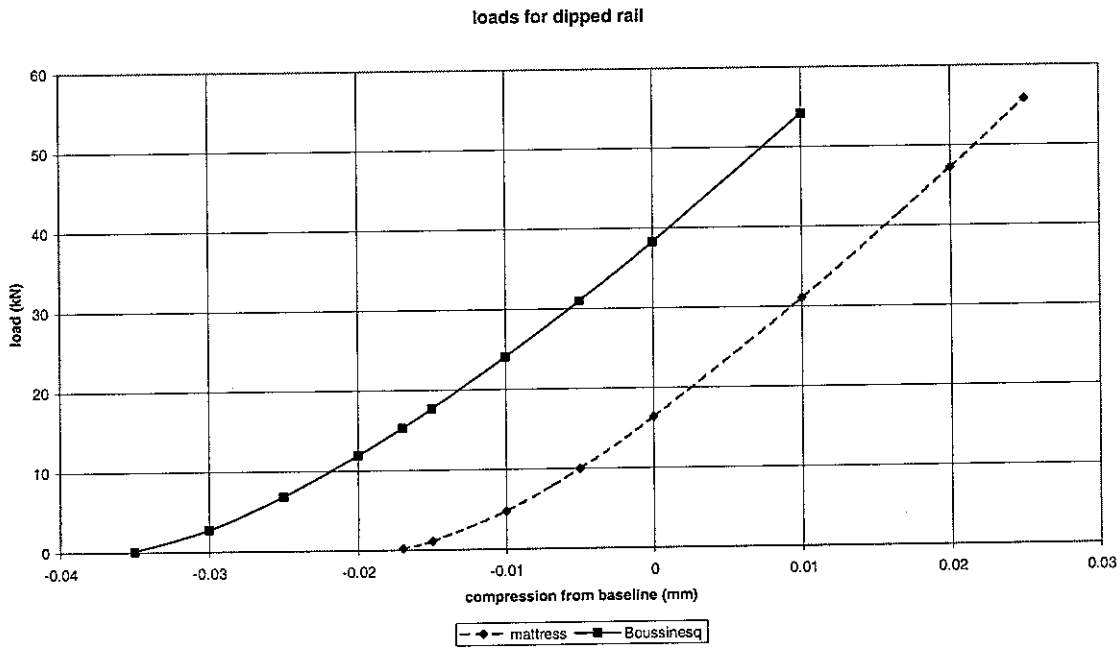

Figure 30. Load-deflection curves for wheels centrally aligned on a cusp. Positive deflection represents compression.

The results in Figure 31 are for a position offset by 1 mm from the point of the cusp. These show a slight kink in the load-deflection behaviour. This behaviour is similar for the two models. The horizontal offset between the two curves is also similar for this case to that in Figure 30. These results suggest that the effects of the half-sized wheel introduced in the mattress model are negligible.

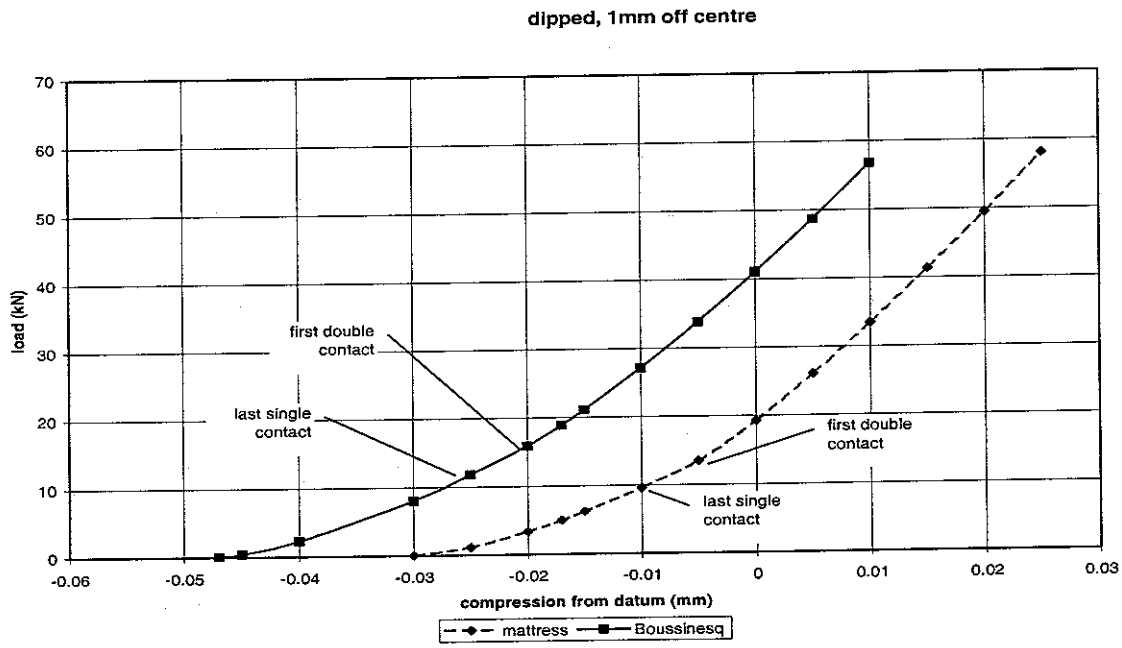

Figure 31. Load-deflection curves for wheels offset 1mm from point of a cusp. Positive deflection represents compression.

7.4 Equivalent roughness and contact patch lengths

The Boussinesq and 2-D mattress models have also been used in the mode of a constant load to obtain the 'equivalent roughness' for the dip shown in Figure 26. The 0.5 mm mesh size has been used. These are compared with the output from the geometrical filter described in Section 3.3, which is given analytically for this dip in Appendix A. The equivalent roughness has a similar form to the dip in Figure 26, starting at +3 mm, but it has a minimum slightly greater than 0, as noted above.

Figure 32 shows results from the Boussinesq model for two different loads (30 and 50 kN). These results concentrate on the region close to the cusp. In each case the static deflection of the contact spring on a flat rail has been removed from the results. Also shown are the original geometry (from Figure 26) and the results from the geometrical filter, which correspond to 0 kN load. It can be seen that the contact spring causes a rounding of the cusp in addition to the reduced depth of the whole feature caused by the geometric filter effect. The rounding occurs over a greater length for a higher load.

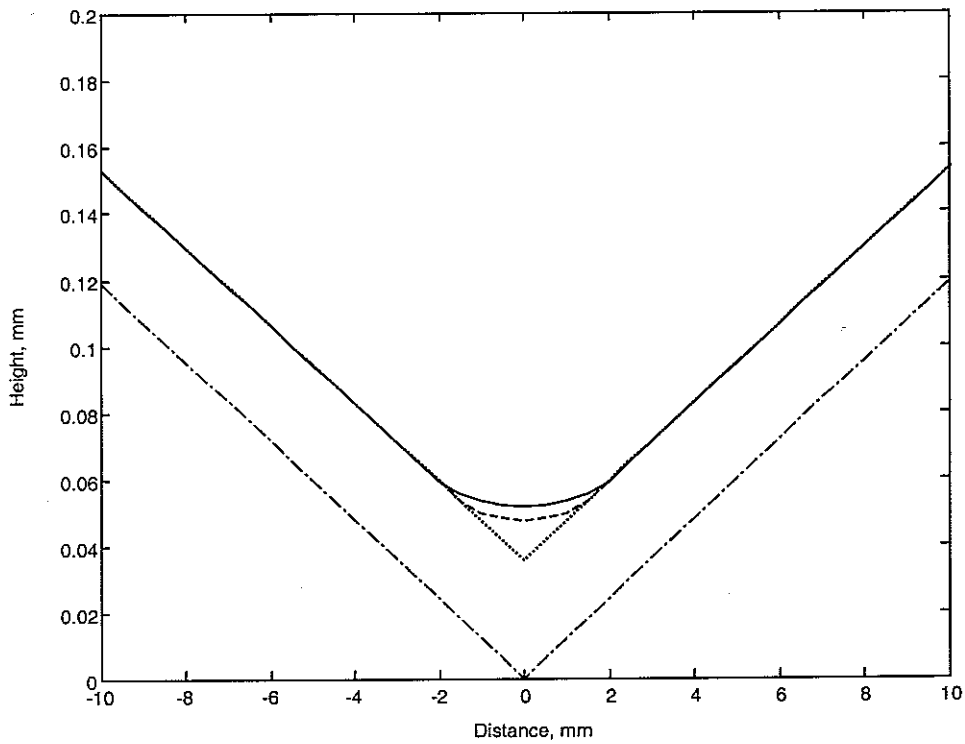

Figure 32. Equivalent roughness from Boussinesq model. ——50 kN load, - - - 30 kN load, ····· geometrical filter, i.e. 0 kN load (from Appendix A), – · – · original geometry.

In Figures 33 and 34 the extent of the contact area, as predicted by the Boussinesq model, is shown for different longitudinal positions of the wheel on the dipped rail. Thus, for each position of the wheel centre relative to the dip (0 is above the cusp of the dip), the shaded region indicates the maximum extent of the contact patch relative to the position on the track. The horizontal dotted line indicates the position of the cusp. The two figures correspond to different values of wheel load (50 and 30 kN respectively). These figures show that no contact is made with the central region of the dip at these wheel loads, see also Figures 28 and 29. Also shown, by the two dashed lines, is the extent of the contact on a flat rail. On the

approach to the dip the contact is shifted back on the rail and after the dip it is shifted forwards, as seen previously in Figures 28 and 29. Some of the results appear slightly erratic due to the discretization used for the contact patch.

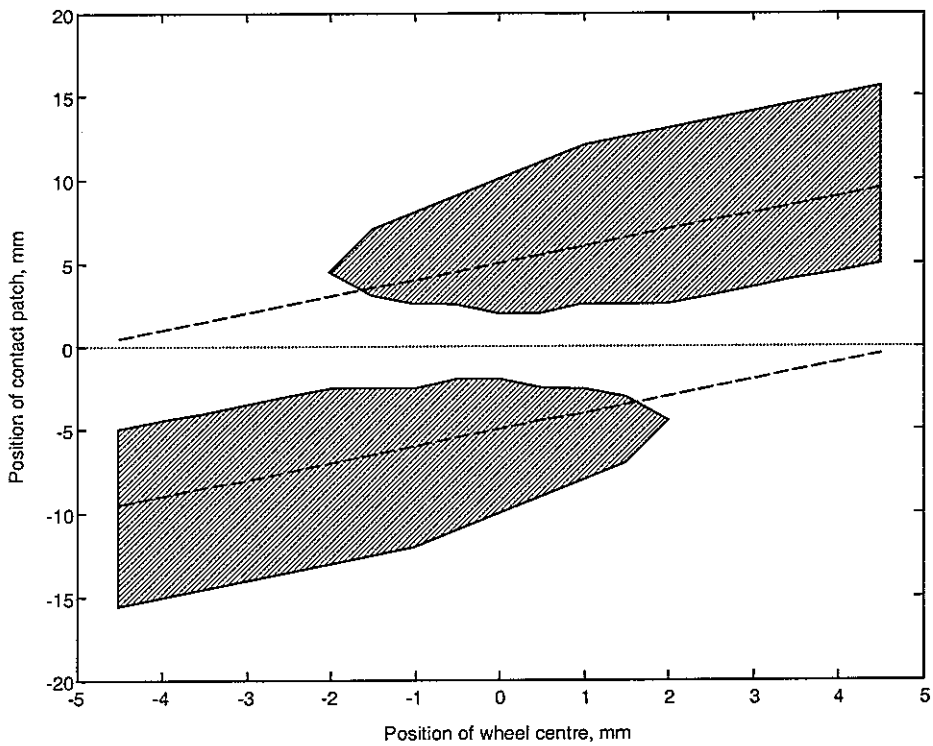

Figure 33. Positions of the contact area from Boussinesq model for 50 kN load at different positions of wheel across the dip. ——dipped rail, - - - flat rail.

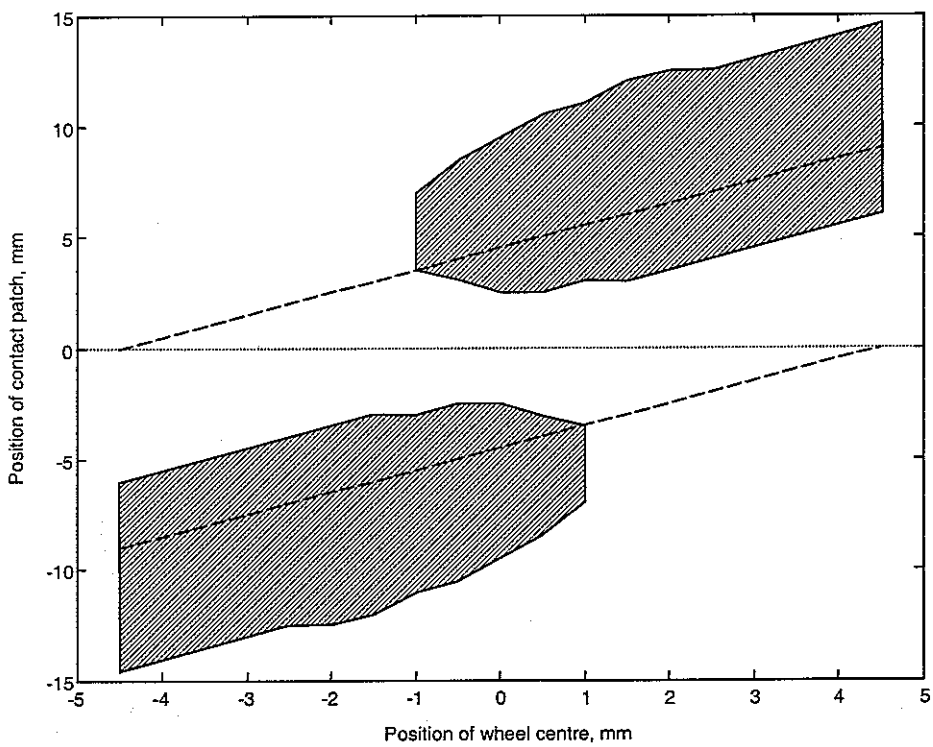

Figure 34. Positions of the contact area from Boussinesq model for 30 kN load at different positions of wheel across the dip. ——dipped rail, - - - flat rail.

Figure 35 shows equivalent roughness results obtained from the mattress model. Here the geometrical filter (0 kN load result) has a smaller effect on the dip than in Figure 32 due to the use of the reduced wheel radius. However, the mattress model introduces slightly greater rounding of the cusp than the Boussinesq model (Figure 32).

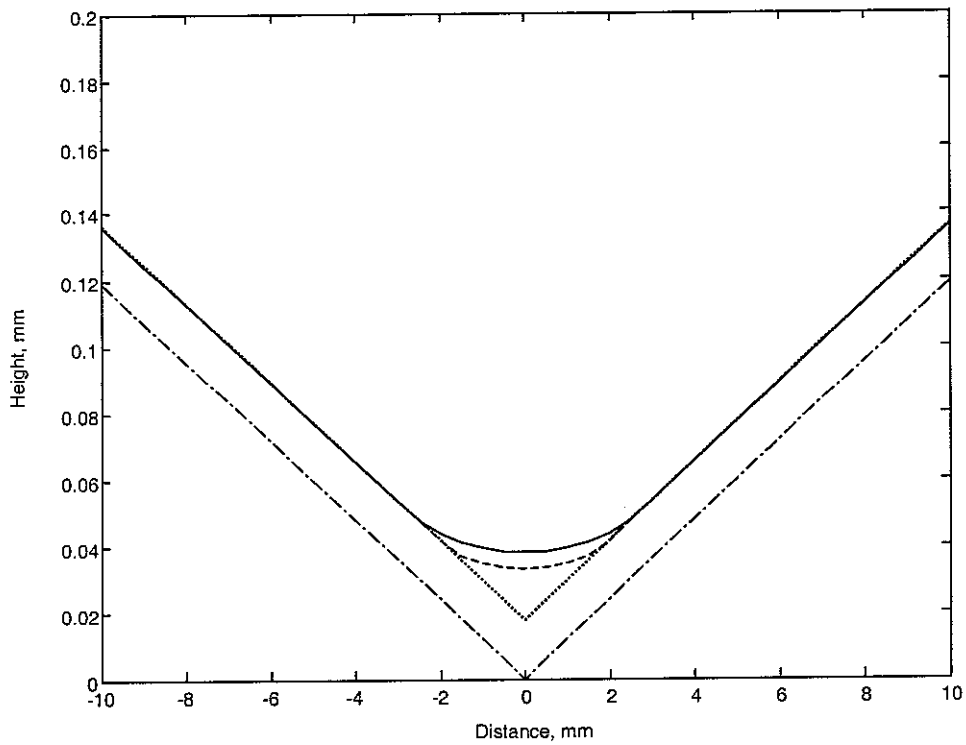

Figure 35. Equivalent roughness from mattress model. ——50 kN load, - - - 30 kN load, ····· geometrical filter, i.e. 0 kN load (from Appendix A), – · – · original geometry.

The extent of the contact patch is shown in Figures 36 and 37 for the mattress model. Although the contact patch length is arranged to be the same for this and the Boussinesq model on a flat rail, in the region of the cusp it is elongated less here than it is for the Boussinesq model (Figures 33 and 34). On the other hand the region with no contact in the centre of the dip, seen for the Boussinesq model, does not occur for the mattress model.

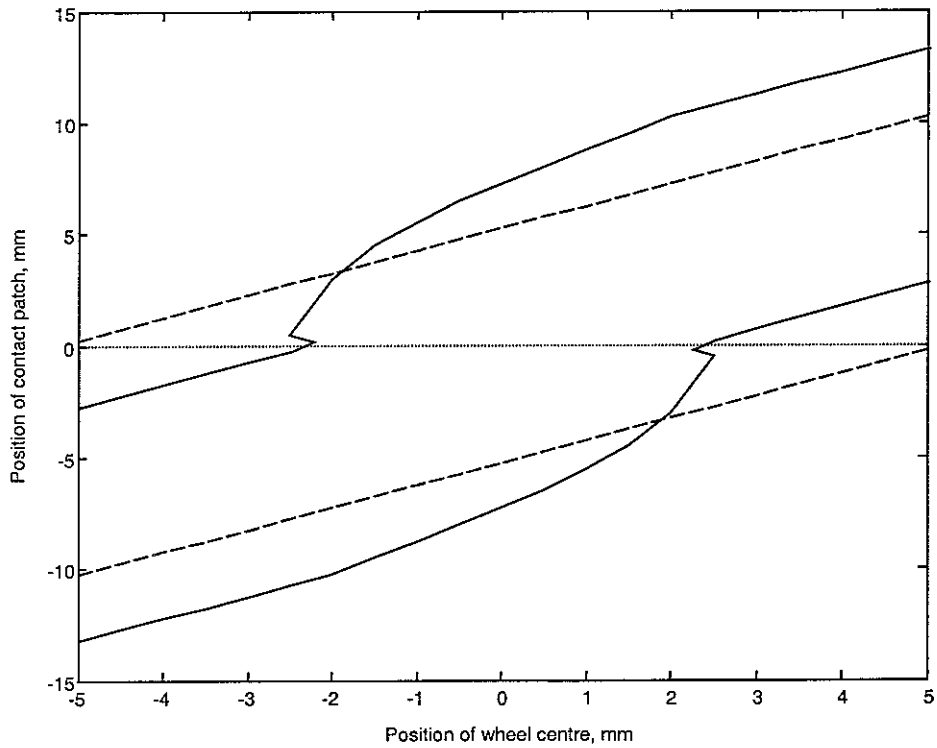

Figure 36. Positions of the contact area from mattress model for 50 kN load at different positions of wheel across the dip. ——dipped rail, - - - flat rail.

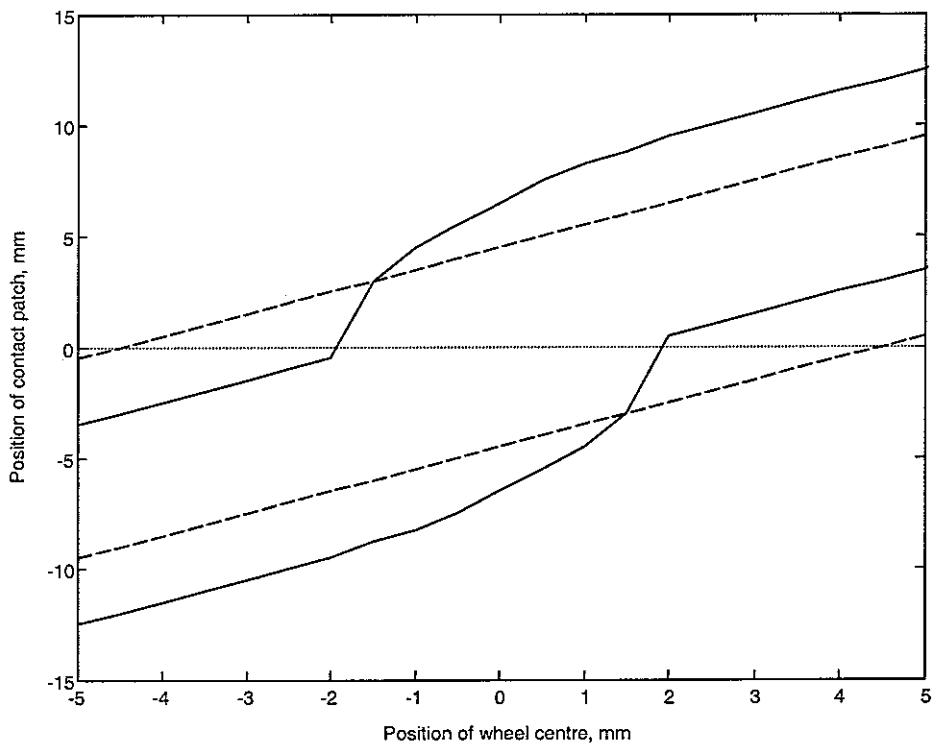

Figure 37. Positions of the contact area from mattress model for 30 kN load at different positions of wheel across the dip. ——dipped rail, - - - flat rail.

Finally, taking the whole 1 m long dipped profile of Figure 26 and the corresponding filtered profiles obtained using the Boussinesq and mattress models, the Fourier transform of these profiles has been taken and converted into one-third octave bands. By forming the difference relative to the raw input an estimate is obtained of the filtering effect. The results are given in Figure 38, plotted against the non-dimensional spatial frequency used earlier, based as before on the contact patch length of the wheel on a *flat* rail.

Compared with the results for sinusoidal roughness in Figure 23, the filter effect here shows some differences. Firstly, the dips do not occur at a non-dimensional frequency of 1, 2, etc but at rather higher frequencies. So, although the contact patch is *elongated*, the frequency of the dip corresponds to a wavelength that is *shorter* than the contact patch length for contact on a flat rail. Secondly, the attenuation at high frequencies is not as large as seen for sinusoidal roughness. Thirdly, the results from the mattress model differ from those of the Boussinesq analysis for non-dimensional spatial frequency between about 1 and 2. At higher frequency, however, the level of attenuation is similar for the two models.

Overall the differences between the Boussinesq and mattress models are not great, indicating that the mattress model could be used fairly reliably. However, the frequency domain filter effect determined from sinusoidal roughness (Figure 23), shown here for comparison, cannot be used for the dipped rail profile. Unlike the case of sinusoidal roughness, the results are also load-dependent even when plotted against non-dimensional spatial frequency.

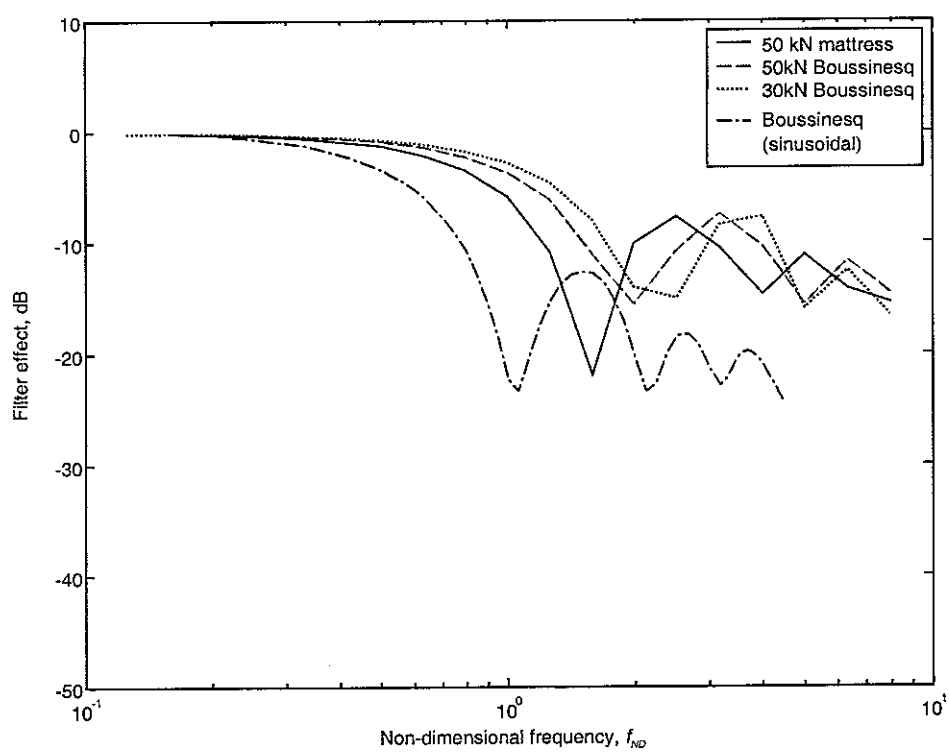

Figure 38. Contact filter effect obtained on a dipped rail.

8 IMPLEMENTATION OF MATTRESS MODEL IN TIME-DOMAIN WHEEL/RAIL INTERACTION MODEL

In order to implement the two-dimensional mattress contact filter in the time-domain wheel/rail interaction model of [4-6], it has to be recast so that a contact force is returned for a given position of wheel and rail. This involves solving equation (18) directly, rather than its inverse (which was solved iteratively), with δ representing the difference between the wheel and rail displacements.

This has been implemented into an interaction model in which the wheel is modelled by its unsprung mass, a 'modal' spring and a small mass at the contact of 3 kg. The rail is represented by a fourth order state-space model as in [4, 5].

8.1 Dynamic results using roughness inputs

The model was used initially with typical surface roughnesses corresponding to a block-braked wheel roughness and a corrugated rail roughness. The block-braked wheel roughness corresponds to a train speed of 100 km/h and the corrugated rail roughness corresponds to 140 km/h. These spectra are shown in Figure 39.

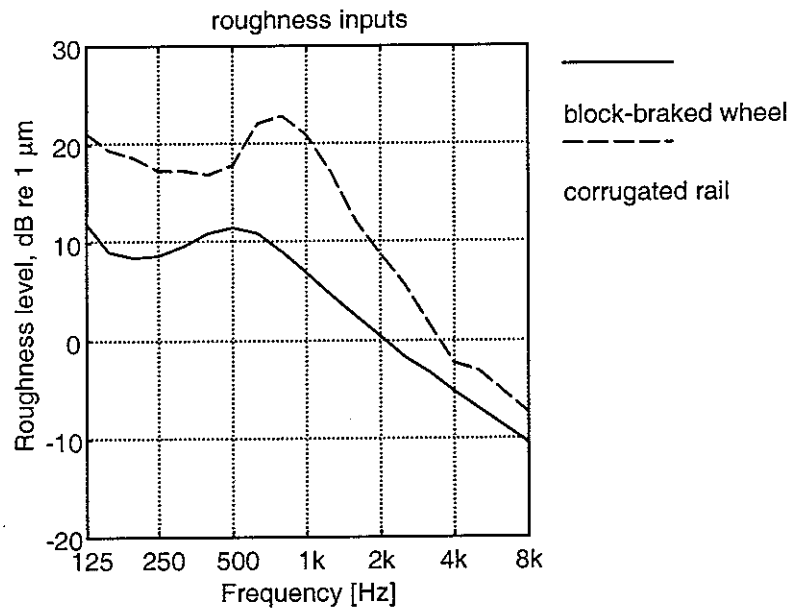

Figure 39 Roughness spectra used to evaluate effect of contact filter.

In each case the unfiltered roughness spectrum was converted into a time series by assuming that all narrow-band components within a one-third octave band have equal power, and then performing an inverse Fourier transform with random phase.

These time series have been filtered using the 2D quasi-static mattress model of Section 2 for different wheel loads. The dynamic model was run (a) with these filtered roughnesses with no contact filter in the interaction model and (b) with the unfiltered roughnesses but including the contact filter in the program. The contact filter effect is calculated by taking the difference between the results from these two runs and adding it to the contact filter effect obtained from the quasi-static contact filter (i.e. the difference in the inputs used). Separate results are shown based on the contact force, rail vibration or the wheel vibration. The results are shown in

Figure 40. The results from applying the quasi-static contact filter (Section 2) to these roughness profiles are also shown.

For a train speed of 100 km/h, the non-dimensional frequency f_{ND} has a value of unity at 3.3 kHz for 25 kN load and 2.1 kHz for 100 kN load. At 140 km/h these frequencies increase to 4.6 and 2.9 kHz. These can be seen to correspond to the first dip in the filter effects in Figure 40.

From these results it can be seen that similar trends are present in each case, but that the result from the contact force differs from that obtained from the wheel or rail responses. Some of the discrepancies between the different dynamic results at high frequencies may be due to inadequacies in the time-stepping calculation. It is seen that, for the higher amplitude roughness (corrugated rail), the results deviate from those of the earlier quasi-static contact filter. This is probably due to the presence of non-linear effects in the wheel/rail interaction force at high amplitudes.

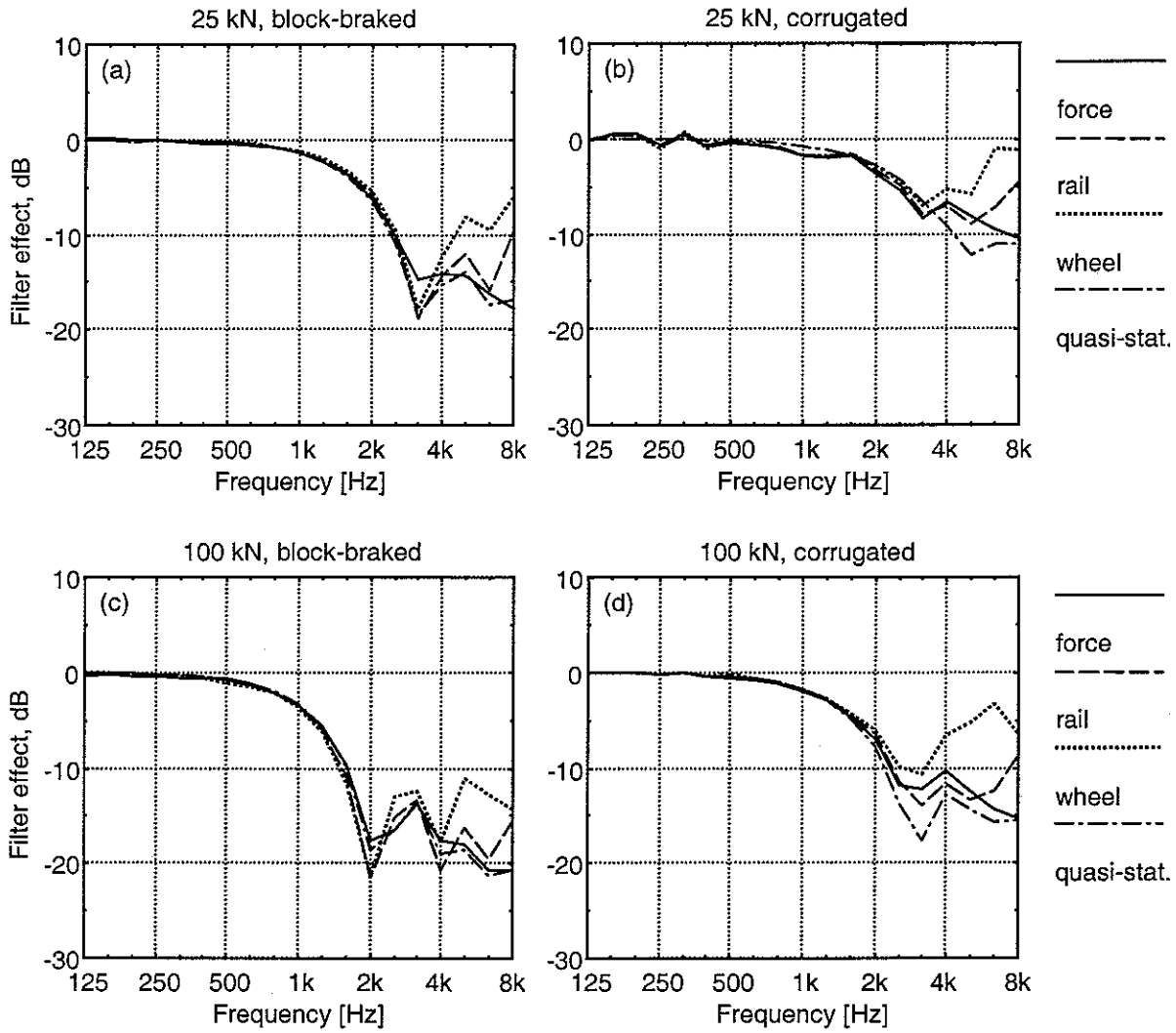

Figure 40 Effect of introducing contact filter into dynamic model using roughness data. (a) For block-braked wheel roughness at 100 km/h, 25 kN load. (b) For corrugated rail roughness at 140 km/h, 25 kN load. (c) For block-braked wheel roughness at 100 km/h, 100 kN load. (d) For corrugated rail roughness at 140 km/h, 100 kN load.

8.2 Dynamic results using dipped rail input

The model was next used with a 3 mm dipped rail profile, as shown in Figure 26. The dynamic model was run (a) with these profiles with no contact filter in the interaction model and (b) with the same profiles but including the contact filter in the program. In each case the train speed was 100 km/h. The contact filter effect is calculated by taking the difference between the results from these two runs. As above, separate results are shown based on the contact force, rail vibration or the wheel vibration. The results are shown in Figure 41 for three values of wheel load.

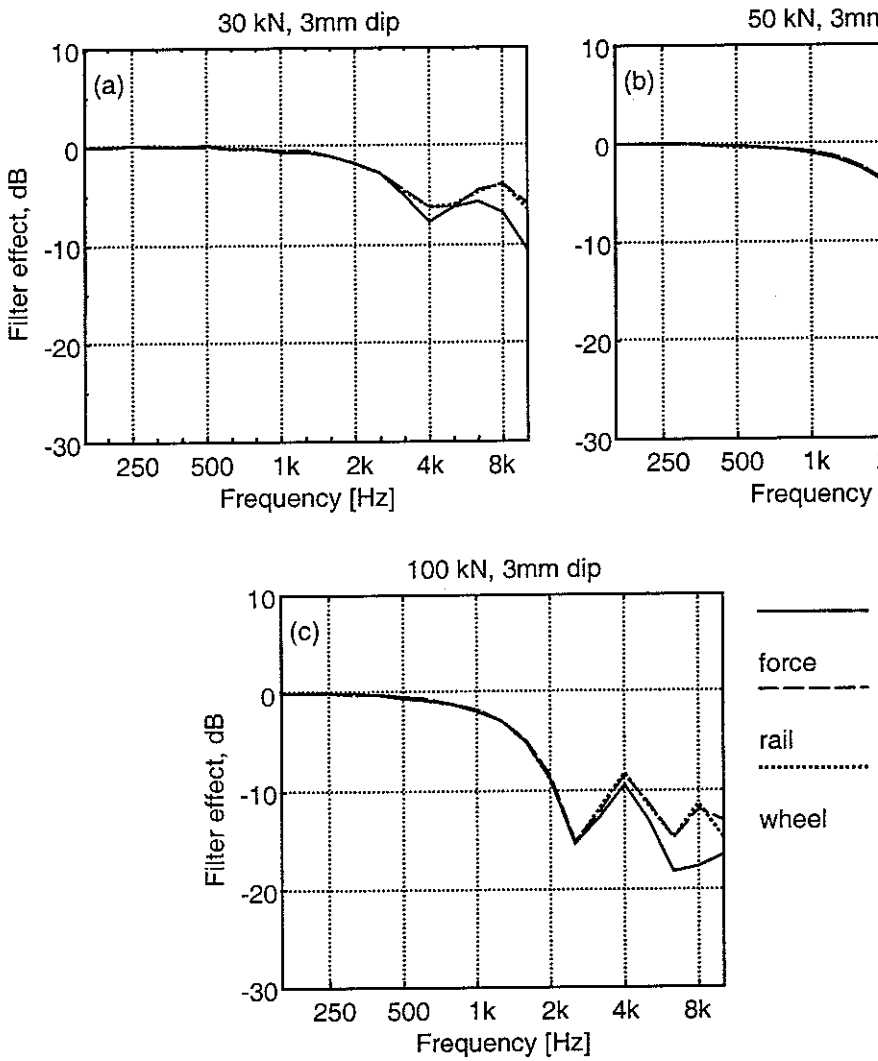

Figure 41 Effect of introducing contact filter into dynamic model using 3 mm dipped rail profile at 100 km/h. (a) For 30 kN load. (b) For 50 kN load. (c) For 100 kN load.

For a train speed of 100 km/h, the non-dimensional frequency f_{ND} has a value of unity at 3.1 kHz for 30 kN load, 2.6 kHz for 50 kN load and 2.1 kHz for 100 kN load. Comparing these values with the filter effects in Figure 41 it can be seen that the first dip occurs at a frequency slightly greater than $f_{ND} = 1$, as seen earlier in the quasi-static results (see Figure 38).

The extent of the filter effect found in these calculations reduces as the static wheel load reduces. This is linked to the greater presence of non-linearities for lower wheel loads: at 30 kN nominal load the wheel loses contact completely for about 15 ms, at 50 kN it unloads momentarily while at 100 kN the contact force does not fall below 50 kN.

9 CONCLUSIONS

A two-dimensional mattress model of elastic contact has been developed. It has been shown that it can be used to represent the contact filter effect between a wheel and a rail. However, it is necessary to adjust the wheel radius in order to ensure the correct contact patch length for a given wheel load and static deflection. Results agree with those from a three-dimensional DPRS model with a maximum discrepancy of 5 dB and an average difference of less than 2 dB.

A Boussinesq model of a concentrated contact has been successfully implemented in Matlab. Results of the Boussinesq model have been compared with a 2-dimensional mattress model and a simple rectangular window. Overall this work shows that under the conditions evaluated, the mattress model is likely to give a good estimate of the behaviour predicted by the more complete Boussinesq model, with no significant bias; results in one-third octave bands are found to be within 3 dB of those from the Boussinesq model.

A simple rectangular window gives a similar filtering effect to the mattress model for sinusoidal inputs. Under some conditions it may be convenient to use the rectangular window. However, the rectangular window may not be used on isolated features such as a dipped rail. Remington's analytical model has also been evaluated and found to give too large an attenuation at high frequencies. A similar conclusion was reached from a comparison with the DPRS model [3].

The filter effect on a dipped rail joint has also been investigated using both the Boussinesq model and the 2-D mattress model. The two models agree well here too. However, it is noted that the filter effect is quite different from that obtained for sinusoidal roughness of moderate amplitude.

The 2-D mattress model only requires a single roughness input profile and can be readily included into a time-stepping model of wheel/rail interaction. When this is done it is found that similar results are obtained to those from the quasi-static filtering of roughness if moderate roughness amplitudes are present. However, with large amplitudes where non-linear effects are significant, including dipped rail joints, the dynamic model gives different results at high frequencies.

REFERENCES

1. P.J. Remington 1987 Wheel/rail rolling noise, I: Theoretical analysis. *Journal of the Acoustical Society of America* **81**, 1805-1823.
2. P.J. Remington and J. Webb 1996 Estimation of wheel/rail interaction forces in the contact area due to roughness. *Journal of Sound and Vibration* **193**, 83-102.
3. D.J. Thompson 2003 The influence of the contact zone on the excitation of wheel/rail noise. *Journal of Sound and Vibration* **267**(3), 523-535.
4. T.X. Wu, D.J. Thompson 2000 Theoretical investigation of wheel/rail non-linear interaction due to roughness excitation. *Vehicle System Dynamics* **34**(4), 261-282.
5. T.X. Wu, D.J. Thompson 2002 A hybrid model for the noise generation due to railway wheel flats. *Journal of Sound and Vibration* **251**(1), 115-139.
6. T.X. Wu, D.J. Thompson 2003 On the impact noise generation due to a wheel passing over rail joints. *Journal of Sound and Vibration* **267**(3), 485-496.
7. K.L. Johnson 1985 *Contact Mechanics,* Cambridge University Press, Cambridge.
8. D.J. Thompson 1990 Wheel/rail noise: theoretical modelling of the generation of vibrations. PhD thesis, University of Southampton.
9. R.B. Randall 1987 *Frequency Analysis*, Bruel and Kjaer, ISBN 87 87355 07 8
10. D.J. Thompson 1996 On the relationship between wheel and rail surface roughness and rolling noise. *Journal of Sound and Vibration*, **193**(1), 149-160.
11. O.R.E.: Wheel/rail contact noise - an experimental comparison of various systems for measuring the rail roughness associated with train rolling noise, Question C163, Railway Noise, Report RP9, Utrecht, 1988.

APPENDIX A Geometry of a wheel on a quadratic dip

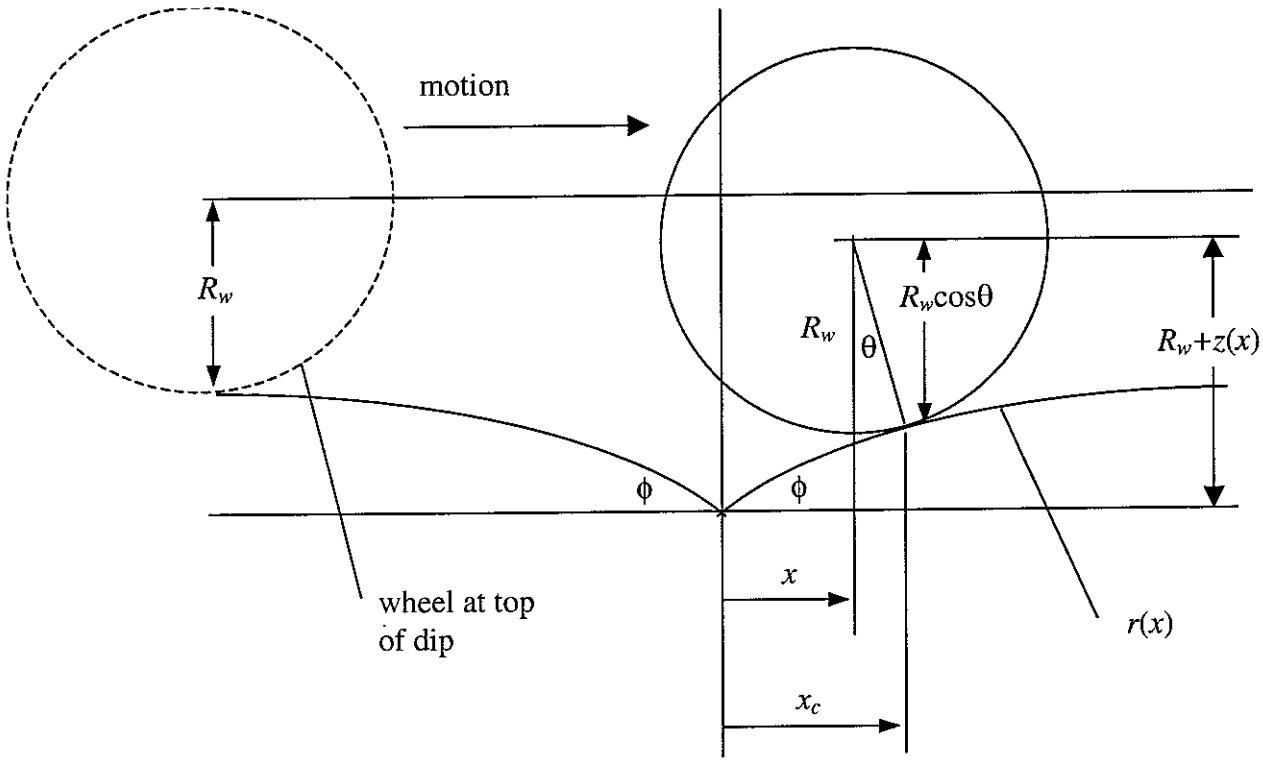

Figure A1 Geometry of a wheel on a quadratic dip.

The wheel of radius R_w is assumed to roll over the rail geometry $r(x)$ defined by the quadratic function

$$r(x) = 2h\left(\frac{|x|}{l}\right) - h\left(\frac{x}{l}\right)^2 \tag{A1}$$

which satisfies $r(\pm l) = h$, $r(0) = 0$. Assuming the wheel to be a rigid circular body, the change in height of its centre relative to the undipped rail, $z(x)$, is a modified form of (A1). For a wheel with radius $R_w \to 0$, $z(x) \approx r(x)$.

When the wheel centre is at x, the contact point is at x_c. These are linked by the angle θ, which is also equal to the slope of the rail profile, $\theta \approx r'(x_c)$.

$$x = x_c - R_w \sin\theta = x_c - R_w r'(x_c) \tag{A2}$$

The height of the wheel centre $z(x)$, which is positive upwards, can be found as

$$z(x) + R_w = r(x_c) + R_w \cos\theta \tag{A3}$$

which gives

$$z(x) \approx r(x_c) - \tfrac{1}{2} R_w \theta^2 \tag{A4}$$

Now, from (A1),

$$\frac{dr}{dx} = \frac{2h(l-x)}{l^2} \text{ for } x \geq 0 \tag{A5a}$$

$$\frac{dr}{dx} = -\frac{2h(l+x)}{l^2} \text{ for } x \leq 0 \tag{A5b}$$

(Note that dips are often defined by the change in angle at the cusp, 2ϕ, where $\phi = r'(0_+) = 2h/l$). Thus, for $x \geq 0$, from (A2)

$$x = x_c - R_w \frac{2h(l-x_c)}{l^2} \tag{A6}$$

or, rearranging

$$x_c = \frac{\left(x + 2R_w \frac{h}{l}\right)}{\left(1 + 2R_w \frac{h}{l^2}\right)} \text{ for } x \geq 0 \tag{A7}$$

Also, from (A4)

$$z(x) \approx 2h\left(\frac{x_c}{l}\right) - h\left(\frac{x_c}{l}\right)^2 - 2R_w h^2 \left(\frac{(l-x_c)}{l^2}\right)^2 \text{ for } x \geq 0 \tag{A8}$$

or

$$z(x) \approx -2R_w\left(\frac{h}{l}\right)^2 + 2\left[2R_w\left(\frac{h}{l}\right)^2 + h\right]\left(\frac{x_c}{l}\right) - \left[2R_w\left(\frac{h}{l}\right)^2 + h\right]\left(\frac{x_c}{l}\right)^2 \text{ for } x \geq 0 \tag{A9}$$

Substituting from (A7), it can be shown that

$$z(x) \approx \frac{1}{1+\left(\frac{2R_w h}{l^2}\right)}\left\{\left(\frac{2R_w h^2}{l^2}\right) + 2h\left(\frac{x}{l}\right) - h\left(\frac{x}{l}\right)^2\right\} \text{ for } x \geq 0 \tag{A10}$$

Thus the motion of the wheel centre has a similar form to the rail profile $r(x)$, but its amplitude is slightly reduced by the leading factor. The value of z at $x = l$, $z(l) = h = r(l)$, but the minimum value at $x = 0$ is greater than 0, *i.e.*

$$z(0) = \frac{\left(\frac{2R_w h^2}{l^2}\right)}{1+\left(\frac{2R_w h}{l^2}\right)} = \frac{2R_w h^2}{l^2 + 2R_w h} \tag{A11}$$

This means that the depth of the rail dip has been reduced from h to $h - z(0)$, a reduction by a factor of

$$\frac{h-z(0)}{h} = 1 - \frac{2R_w h}{l^2 + 2R_w h} = \frac{l^2}{l^2 + 2R_w h} \tag{A12}$$

The gradient of $z(x)$ is given by

$$\frac{dz}{dx} = \frac{1}{1+\left(\frac{2R_w h}{l^2}\right)} \left\{ 2\left(\frac{h}{l}\right) - 2h\left(\frac{hx}{l^2}\right) \right\} \text{ for } x \geq 0 \tag{A13}$$

which at $x = 0_+$ has a value of

$$\frac{dz}{dx} = \frac{2\left(\frac{h}{l}\right)}{1+\left(\frac{2R_w h}{l^2}\right)} \text{ for } x = 0_+ \tag{A14}$$

This is less than the slope of r at $x = 0$ ($2h/l$). Thus the change in slope experienced by a wheel of radius R_w is slightly less than 2ϕ, again by the factor given in equation (A12).